ISSN 1732-9353 (suspended)
eISSN 2543-7496

Scientific Review

Engineering and Environmental Sciences

Przegląd Naukowy
Inżynieria i Kształtowanie Środowiska

Vol. 31 (3) 2022 Issue 97
Quarterly

SCIENTIFIC REVIEW
ENGINEERING AND ENVIRONMENTAL SCIENCES
Quarterly

EDITORIAL OFFICE ADDRESS
Wydział Budownictwa i Inżynierii Środowiska SGGW, ul. Nowoursynowska 159, 02-776 Warsaw, Poland
tel. (+48 22) 59 35 363, 59 35 210, 59 35 302
e-mail: srees@sggw.edu.pl
https://srees.sggw.edu.pl

ISSN 1732-9353 (suspended)
e-ISSN 2543-7496

Electronic version of the Scientific Review Engineering and Environmental Sciences is primary version

All papers are indexed in the data bases as follows: AGRO(Poznań), BazTech, Biblioteka Nauki, **CrossRef**, **DOAJ**, **Google Scholar**, **Index Copernicus**, INFONA, POL-Index, **SCOPUS**, SIGŻ(CBR)

Scientific Review

Engineering and Environmental Sciences

Przegląd Naukowy

Inżynieria i Kształtowanie Środowiska

Vol. 31 (3) 2022 Issue 97

Contents

Wydawnictwo SGGW, Warsaw 2022

Wydawnictwo SGGW wydawnictwosggw

Editorial work – Anna Dołomisiewicz, Violetta Kaska

ISSN 1732-9353 (suspended) eISSN 2543-7496

Scientific Review Engineering and Environmental Sciences (2022), 31 (3), 149–160

Sci. Rev. Eng. Env. Sci. (2022), 31 (3) https://srees.sggw.edu.pl

ISSN 1732-9353 (suspended) eISSN 2543-7496 DOI 10.22630/srees.2971

Received: 29.04.2022
Accepted: 21.06.2022

Thomas Terna AULE[1, 2] ✉ https://orcid.org/0000-0003-2100-4951

Roshida Binti Abdul MAJID[1]

Mahmud Bin Moh'd JUSAN[1]

[1] Universiti Teknologi Malaysia, Faculty of Built Environment and Surveying, Malaysia
[2] Federal Polytechnic Kaura Namoda, School of Environmental Studies, Nigeria

EXPLORING CULTURAL VALUES AND SUSTAINABILITY PREFERENCES IN HOUSING DEVELOPMENT: A STRUCTURAL EQUATION MODELING APPROACH

Key words: indigenous housing, cultural values, sustainable development, sustainability preferences, Tiv housing

Introduction

Sustainability may be seen as behaviors and procedures directed toward meeting our present needs without jeopardizing the requirements of subsequent generations (United Nations SDGs, 2015). Environment, as one of the primary pillars of sustainability, covers the provision of suitable housing and the creation of human settlements that are inclusive, safe, resilient, and long-lasting (Car-Pušić, Tijanić, Marović & Mladen, 2020). This inclusiveness means that essential services should be provided through changes, improvements, and slum upgrading for the growth of both countries, communities, and regions. According to Neef et al. (2018), this embraces giving communities value-based developments to retain their identities, adapt to climate change, and keep their cultures alive.

Furthermore, to ensure inclusiveness, end-users as beneficiaries should be involved in the planning, designing, and developing implementation schemes in their areas (Wang, Zhao, Wu & Tang, 2017; Ostańska, 2019). The integration of participatory strategy is vital in ensuring the value-based development proponent and preservation of people's cultural identities in accordance with the UN Sustainable Development Goals

✉thomas1979@graduate.utm.my

(SDGs) (Ezennia & Hoskara, 2021; Aule, Majid, Jusan & Ayoosu, 2022). The position of the SDGs is that stakeholders must ensure that local communities have a say in the planning and management of infrastructures in their areas (UN General Assembly, 2016; Aule, Jusan & Ayoosu, 2019). This call for participation further justifies the need for appropriate articulation of cultural values and sustainable development in the built environment.

Nigerian stakeholders, like other developing economies, are building value-based housing and urban development identity from the country's more than 250 ethnic groups (Isah & Khan, 2016; Umar, Yusuf, Ahmed & Usman, 2019). A study by Maina (2013) revealed that previous mass housing arrangements that failed to take people's values into account during planning and designing resulted in "uncomfortable prototypes" where inhabitants made unprotected changes in order to merge their mainstream cultural beliefs. One may ask, what is the relationship between the cultural values of the different Nigerian ethnic groups and their preferences for sustainable housing improvements in their indigenous built environments?

Therefore, this study assumes that there is a significant relationship between values and preferences for sustainable housing development. With the significant relationship, it is becoming increasingly important to examine the inherent values that motivate the indigenous housing of the numerous cultural groups in Nigeria so that all-encompassing vernacular architecture suitable to most groups may be articulated and implemented. Besides, the primitive native values will serve as reliable data for justified value-based scheduling, creating, and developing projects with distinctive identities consistent with present-day advancements.

The hypothesized significant association between cultural values and the people's preferences for sustainable housing improvements will be tested in this study using the structural equation modelling (SEM) approach. The ordinal-scale survey for this study was carried out between February and March 2022 to systematically validate the values in indigenous built surroundings of the Tiv society of Benue State, central Nigeria, and relate them to the people's preferences for lasting transformational improvements. The research surveyed and tested the link between people's values and their choices for sustainable development by utilizing factors previously discovered through some qualitative inquiries. The result is intended to give helpful information for value-based strategies, designs, and implementation among the Tiv society in central Nigeria. Furthermore, the findings will be articulated with the values of other ethnic groups to establish an acceptable and comprehensive vernacular architecture and urban identity acceptable to most Nigerians.

Material and methods

Content design of the survey

This part of the study was a cross-sectional ordinal-scale survey conducted between February and March 2022 using online Google form instruments. The study collected quantitative data to statistically establish the mainstream values and test their relationship with the transformative preferences of the Tiv people of central Nigeria. The survey variables for the inquiry were obtained from themes elicited in previous interviews, as summarized in Figure 1.

FIGURE 1. Elicited attributes, consequences, and values in Tiv indigenous housing. Adapted as published by the authors (Aule et al., 2022)

The elicited variables earlier coded into attributes, consequences, and values using the QSR® NVivo® software version 12 were also ranked based on the frequency of mentions by interview participants, as presented in Table 1. The elicited and ranked variables provided the basis for the subsequent ordinal scale survey, which is the primary methodology for this study. The variables tested to be significant and valid with 20% frequency in the previous study were further investigated employing a five-point Likert scale, with 1 representing "highly disagree" to 5 for "highly agree". The survey questions were categorized into attributes, consequences, values, and preferences for transformative improvements.

Questions were based on the shapes, material, and settings of the peoples' indigenous houses, as earlier elicited and ranked. All questions were formatted multi--choice with a paragraph space provided at the end of the survey for necessary feedback from respondents. The "required" restriction was also activated in the Google form to check cases of missing data. Finally, a survey link was generated and shared with some social media groups and indigent

TABLE 1. Variables elicited from interviews provided the basis for the ordinal scale survey. Adapted as published by the authors (Aule et al., 2022)

Interview attributes				
S/No	Concrete attributes		Abstract attributes	
i	round or circular shape	23	cultural meaning	17
ii	separate houses	22	material availability	15
iii	earth-mud	19	history, heritage	13
iv	bamboo framed roof	18	natural of earth	11
v	disperse setting	18	strengths of material	07
vi	thatched roof	17	drainage of roof	06
vii	reeds, canes	05	infinite earth	05
viii	rectangle shape	04		
Interview consequence				
S/No	Functional consequence		Psycho-social consequence	
i	free movements	15	feeling natural	17
ii	climatic control	12	feeling relaxed	09
iii	farming space	09	feeling modest	07
iv	ventilating space	09	feeling strong	07
v	protective purpose	07	feeling cool	05
Interview values				
S/No	Instrumental values		Terminal values	
i	determination & ambition	16	independent living	17
ii	simple living	14	basic comfort	11
iii	cleanliness	11	safety & security	07
iv	creative craft	11	cultural identity	06
v	nature conservation	09		

individuals in Benue state, the study area. Since the survey is concerned with one state in Nigeria, Benue state was taken as an area cluster where the sample was taken. As an area with limited internet and other electronic amenities, the convenient sampling approach was used where units in the Benue cluster volunteered to engage in the survey. The results were first scrutinized using the IBM® Statistical Package for Social Science (SPSS®) software version 22. Main tests were conducted using the IBM® SPSS® Analysis of Moment Structures (Amos™) software version 24 for the first-order confirmatory factor analysis (CFA) and the subsequent second-order SEM.

An overview of structural equation modeling

While it could be more accessible to measure tangible elements such as the number of people, weight, height, cars, and temperature, among others, with some physical devices; it is often difficult to measure intangible perceptions, values, achievement, esteem, preferences, satisfaction, among others, using instruments (Pahlevan Sharif & Sharif Nia, 2018). The Likert scale is one of the practical ordinal survey tools to measure non-concrete perceptions of people (Kline, 2016). Therefore, the CFA and SEM are instruments to analyze and test correlations in ordinal scale data, especially in social science studies.

The SEM estimates a sequence of dependent connections among a collection of ideas or constructs represented by several measurable variables, incorporating the results into an integrated model (Malhotra, 2020). Though referred to by other family names such as covariance structure analysis, covariance structure modeling, or covariance structure analysis (Kline, 2016), it is usually carried out in two parts called orders. The two parts are the first-order CFA and the second-order SEM. Typically, CFA involves drawing path diagrams and covariances and loading the observed or measured variables called factors. The loaded CFA model is then run and assessed, eliminating insignificant factors with less than 0.5 standardized regression weights (Pahlevan Sharif & Sharif Nia, 2018). The model is then fitted based on recommended standards, with reliability and validity also assessed. The first-order CFA is completed once the model goodness-of-fit is attained and conditions for reliability and validity are met.

The second-other SEM involved reorganizing the model into independent and dependent constructs, fitting it before establishing the strength of their relationships.

Since this study is modeled on constructs of attributes, consequences, and values, the SEM model will be used to test the three hypotheses:

- H_1: There is a significant correlation between housing attributes and transformative preferences.
- H_2: There is a significant correlation between utility consequences and transformative preferences.
- H_3: There is a significant correlation between people's values and transformative preferences.

Demography of survey respondents

This section contains the demography of survey respondents. Regarding age, about 82% of respondents were adults above 30 years with the requisite knowledge

and experience to elicit meaning and values in their indigenous built environments. Concerning the state of origin, close to 98% of respondents were indigenous to Benue state, the study area; however, the remaining 2% of outsiders were retained for negative case analysis and generalizations. In the sphere of home ownership, more than 80% of respondents either live in their houses or rented apartments, while the remaining were drawn from local builders and female leaders. Interestingly, all the respondents reported having completed their secondary education, with about 81% graduates.

The demography of the survey respondents looks good as most seem mature and responsible enough to provide needed responses. Even the 18% of female respondents seem reasonable to identify gender-based values in the African context, where participation of the female gender in many spheres is still gathering momentum.

Preliminary data checks and screening

Two supervisory experts, among other experienced research-group members, validated the survey contents. Their valuable feedback and inputs were utilized to refine and finalize the inquiry. Furthermore, preliminary results for the first week were utilized as a pilot study where inconsistencies were checked and minor errors were corrected. While the sample size for CFA varies based on complexities and area of study, many scholars agreed to a minimum of 200 valid responses (Kline, 2016; Sharif, Mostafiz & Guptan, 2018; Malhotra, 2020; Achoba, Majid & Obiefuna, 2021).

Though 255 completed responses were received, 12 were initially excluded as redundant and outliers. With the "required" restriction in the online survey, there was no incidence of missing values from the data collected. A general reliability test was conducted where data exhibited high consistency with a Cronbach's alpha of 0.934. A principal component analysis (PCA) test was also conducted, with most variables having communalities greater than 0.5 weights. Furthermore, the Kaiser–Meyer–Olkin (KMO) and Bartlett's test of sphericity were generated to check the correlation matrix and data's suitability for a productive confirmatory factor analysis (CFA). As shown in Table 2, the PCA results produced a 0.000 significance level and 0.872 KMO, confirming the relevance of the data set for CFA.

TABLE 2. Kaiser–Meyer–Olkin (KMO) and Bartlett's test of sphericity (own studies)

Test		Value
Kaiser–Meyer–Olkin measure of sampling adequacy		0.872
Bartlett's test of sphericity	chi-square approximation	6 438.240
	degrees of freedom	1 225
	significance	0.000

Following recommendations by scholars (Sharif et al., 2018), an exploratory factor analysis (EFA) was also conducted on the data to check variables with high cross-loadings, where two were finally removed, bringing the absolute sample to 241 valid respondents. With suggestions from the resulted eigenvalues, the constructs were grouped into the four parent clusters of attributes, consequences, values, and preferences.

Aule, T. T., Majid, R. B. A., Jusan, M. B. M. (2022). Exploring cultural values and sustainability preferences in housing development: A structural equation modeling approach. *Sci. Rev. Eng. Env. Sci.*, *31* (3), 149–160. DOI 10.22630/srees.2971

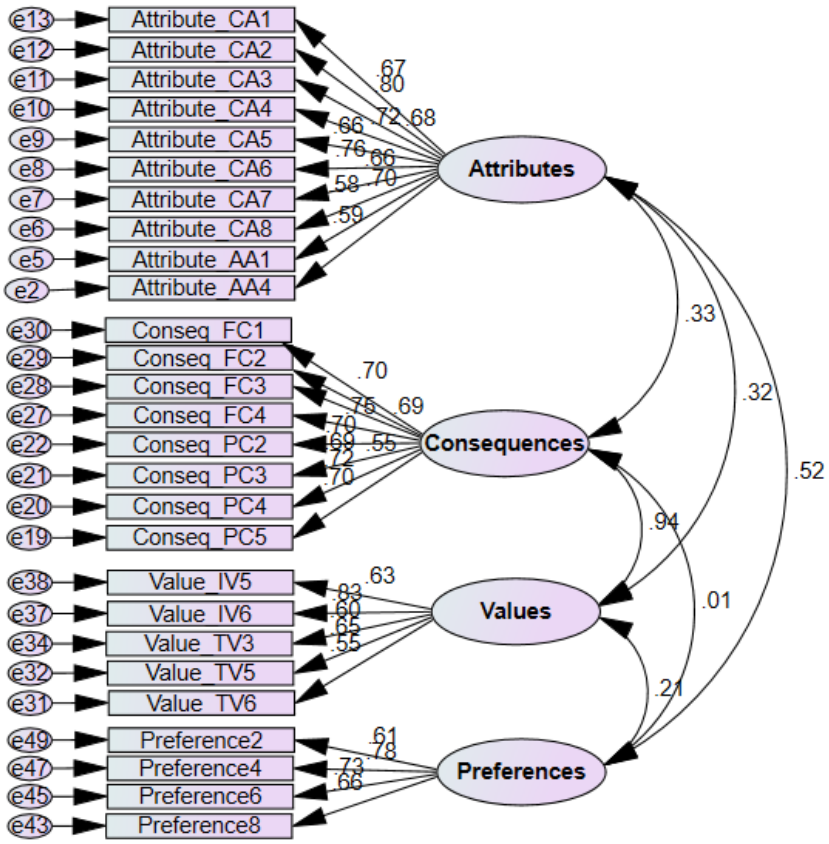

FIGURE 2. Variables with significant factor loadings (own studies)

Results and discussions

The first-order confirmatory factor analysis factor loadings

The IBM® SPSS® Amos™ software version 22 was utilized for the first-order CFA and the subsequent second-order SEM. The CFA commenced with a path diagram drawn with four latent constructs of attributes, consequences, values, and preferences, each with their respective number of observed variables and error terms, as presented in Figure 2.

The observed variables were loaded into the four latent constructs of attributes, consequences, values, and preferences, where 27 of the variables were returned significant, with standardized regression weights of 0.5 and above.

CFA model fit

Variables with weaker loadings were systematically eliminated during the CFA model assessment, while the recommended model fit indices were checked in the output mode. A model fit was eventually realized

TABLE 3. First-order CFA model goodness-of-fit based on recommended indices (own studies)

Goodness-of-fit	Chi-square group			Absolute fit	Incremental fit	Incremental fit	Absolute fit	Standard *RMR*
Fitness indexes	C_{min}	*df*	C_{min}/df	*CFI*	*IFI*	*TLI*	*RMSEA*	*RMR*
Recommended value	> 0.05 sig.		< 3.0	> 0.90	> 0.90	> 0.90	< 0.08	< 0.08
This model	140.426	59	2.380	0.933	0.934	0.912	0.057	0.689

The CFA model is accepted for meeting acceptance levels.

with acceptable indices, as shown in Table 3. Though a perfect CFA model fit should have a significant chi-square value greater than 0.05, the larger-sample hallmark of SEM most times affects its significance (Pahlevan Sharif & Sharif Nia, 2018; Achoba et al., 2021). In line with Kline (2016) and Malhotra (2020), other indices that fit a model's goodness-of--fit index (*GFI*) include comparative fit index (*CFI*), Tucker–Lewis index (*TLI*), normal chi-square per degree of freedom (C_{min}/df), root-mean-square error approximation (*RMSEA*), and standardized root mean square residual (*SRMR*). Table 3 presents the fitted first-order CFA model according to recommendations (Kline, 2016; Pahlevan Sharif & Sharif Nia, 2018; Malhotra, 2020).

Reliability and validity of the CFA model

Reliability refers to how a scale produces consistent results if repeated measurements are made (Malhotra, 2020). In SEM, a construct can be measured with composite reliability (*CR*), maximum reliability [max*R*(*H*)], Cronbach's alpha (α), or omega (ω), where all are expected to have a value greater than 0.70 (Pahlevan Sharif & Sharif Nia, 2018). This model is reliable as all values for constructs' composite, and maximum reliability is above 0.70 acceptable minimum, as shown Table 4.

On the other hand, validity may be seen as the extent to which observed disparities in scale scores represent actual variances between matters on the feature being assessed rather than a systematic or random error (Malhotra, 2020). Two types of validity are measured in SEM: convergent and discriminant. While the convergent validity in SEM can be assessed through average variance extracted (*AVE*), which is expected to be greater than 0.50 for all constructs, the discriminant validity, on the other hand, may be measured as maximum shared variance (*MSV*) expected to be less than the *AVE*. It can also be assessed using heterotrait-monotrait (*HTMT*) measurement, expected to be less than 0.9 for all constructs (Pahlevan Sharif & Sharif Nia, 2018). As presented in Table 4, the reliability and validity of this study's model were generated using Amos™ plugin called Master Validity Tool developed by James Gaskin and John Lim (Gaskin, James & Lim, 2019).

While the convergent *AVE* is generally expected to be viable with values above 0.50 for all constructs, it is viewed by Malhotra (2020) as being too strict a measure for the models validity. Pahlevan Sharif and Sharif Nia (2018) further explain the challenge of attaining all recommended values in new research areas, where knowledge of phenomenon is minimal, with scanty

Aule, T. T., Majid, R. B. A., Jusan, M. B. M. (2022). Exploring cultural values and sustainability preferences in housing development: A structural equation modeling approach. *Sci. Rev. Eng. Env. Sci.*, *31* (3), 149–160. DOI 10.22630/srees.2971

TABLE 4. Analysis of model reliability and validity (own studies)

	CR	*AVE*	*MSV*	max*R*(*H*)	Attribute	Consequence	Value	Preference
Attribute	0.842	0.519	0.261	0.858	0.720	×	×	×
Consequence	0.832	0.624	0.566	0.846	0.228**	0.790	×	×
Value	0.722	0.466	0.566	0.737	0.408***	0.753***	0.683	×
Preference	0.748	0.599	0.261	0.777	0.510***	–0.063	0.275**	0.774

** Values statistically significant at p level < 0.010.

*** Values statistically significant at p level < 0.001.

TABLE 5. The essential attributes, consequences, and values predicting preferences for sustainable housing transformation (own studies)

Construct	Code	Variable	SRW (λ)	Cronbach's alpha (α) > 0.7	Composite reliability (*CR*) > 0.6	Average variance (*AVE*) > 0.5
Attribute	AC2	earth-mud materials	0.697	0.832	0.842	0.519
	AC3	use of sun-dried adobe bricks	0.678			
	AC5	use of thatch roofs	0.594			
	AC6	dispersed compound setting	0.802			
	AA1	expression of culture	0.747			
	AA4	compound expresses communal living	0.667			
Consequence	CF1	insulation from heat and rainfall	0.743	0.875	0.832	0.624
	CF3	simple to construct	0.721			
	CF4	cheap and economical materials	0.800			
	CP2	feel cool within the buildings	0.693			
Value	VI5	simplicity and hospitality	0.618	0.737	0.722	0.466
	VI6	cleanliness & vigilance	0.741			
	VT3	cultural identity	0.659			
	VT5	promote communal unity	0.522			
Transformative preference	Pref2	independence & privacy	0.595	0.747	0.748	0.599
	Pref4	modernize Tiv houses	0.535			
	Pref6	integrate traditional forms in modern	0.684			
	Pref8	context-specific buildings	0.604			

published materials. The study proposes that an *AVE* measure of more than 0.40 and other acceptable measures is deemed sufficient to establish a model's acceptability validity. Accordingly, the 18 constructs that were finally seen to be reliable and valid represent the most important attributes, consequences and values in Tiv indigenous housing, presented in Table 5.

Structural equation model

Structural equation model is the second--order analysis. Most of the variables fitted in the CFA, tested to be reliable with acceptable validity, were utilized for the final structural model and for testing the study hypothesis. The measures for goodness-of-fit such as comparative fit index (*CFI*), Tucker–Lewis index (*TLI*), normal chi-square per degree of freedom (C_{min}/df), root-mean-square error approximation (*RMSEA*), and standardized root mean square residual (*SRMR*), were also attained. Therefore, as presented in Figure 3, the second-order structural model was fit based on recommended indices (Kline, 2016; Pahlevan Sharif & Sharif Nia, 2018; Malhotra, 2020). With the second-order model fulfilling indices for goodness-of-fit, it was used to predict the relationship between the constructs.

Cultural values and sustainability preferences

The squared multiple correlations were seen to have good values for the two endogenous constructs of values

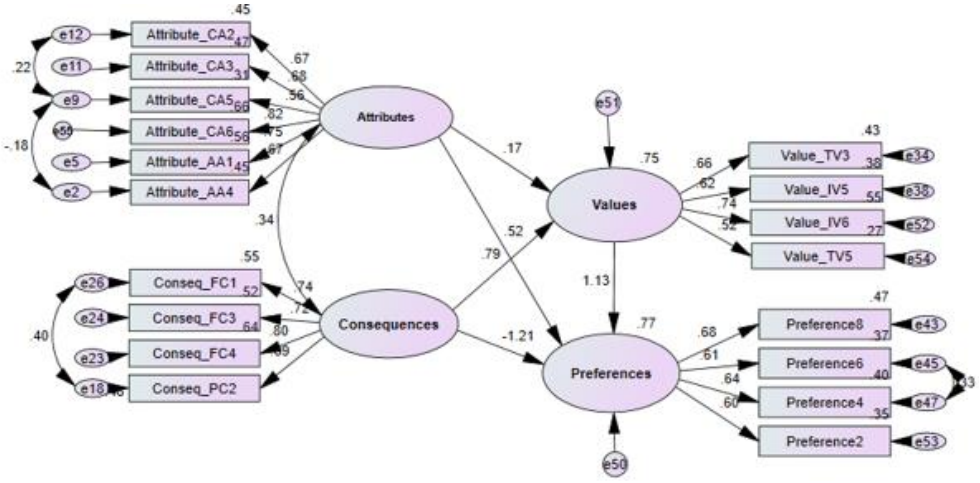

Goodness-of-fit	Chi-square group			Absolute fit	Incremental fit	Incremental fit	Absolute fit	Standard RMR
Fitness indexes	C_{min}	*df*	C_{min}/df	*CFI*	*IFI*	*TLI*	*RMSEA*	RMR
Recommended value	> 0.05 sig.		< 3.0	> 0.90	> 0.90	> 0.90	< 0.08	< 0.08
This model	265.491	125	2.124	0.920	0.916	0.901	0.068	0.693
SEM model is accepted for meeting acceptance level								

FIGURE 3. Model and fitted indices for the second-order SEM (own studies)

Aule, T. T., Majid, R. B. A., Jusan, M. B. M. (2022). Exploring cultural values and sustainability preferences in housing development: A structural equation modeling approach. *Sci. Rev. Eng. Env. Sci.*, *31* (3), 149–160. DOI 10.22630/srees.2971

TABLE 6. Significant regression weights showing valid relationships (own studies)

			Estimate	*SE*	*CR*	*p*	Label
Values	<---	Attributes	0.209	0.085	2.458	0.014	×
Values	<---	Consequences	0.626	0.086	7.276	***	×
Preferences	<---	Attributes	0.600	0.144	4.153	***	H_1
Preferences	<---	Consequences	–0.891	0.244	–3.651	***	H_2
Preferences	<---	Values	1.054	0.329	3.208	0.001	H_3

H_1: Attributes have a significant relationship with sustainability preferences.

H_2: Consequences have a significant relationship with sustainability preferences.

H_3: Values have a significant relationship with sustainability preferences.

and preferences in the second-order SEM. Generally, the SEM model in this study has good squared multiple correlations (R^2) of 0.75 for values and 0.77 for preferences. This correlation means the model explained 75% variance for the values and 77% variances for preferences. The final unstandardized regression weights (*p*-values), showing relationships of the constructs, were all tested significantly, with values less than 0.05. Apart from the consequences construct with a significant but negative correlation with preferences, the two other constructs of attributes, and values, have significant and positive relationships with sustainable preferences.

Therefore, as presented in Table 6, the three research hypotheses, H_1, H_2 and H_3, significantly correlate with preferences for sustainable housing improvements.

Conclusion

Exploring the inherent values in Nigerian indigenous housing is becoming increasingly important to articulate value--based development for identity and cultural sustainability. In this study, the mainstream indigenous housing values for the Tiv society of central Nigeria were elicited through their attributes and consequential utility. This study's subsequent ordinal scale quantitative approach was built on earlier perceptions elicited through laddering interviews. The five-point Likert scale survey data were tested and validated to have reliable results, ranking the most critical attributes, consequences, and values in Tiv indigenous housing. The correlational outcomes show that attributes, consequences, and values significantly affect people's preferences for sustainable, transformative improvements.

Future developments in the area ought to reflect society's mainstream values. Additionally, with the global solidarity to attend to poorer and vulnerable people, efforts should be made by governments, organizations, and highly placed individuals to transform and improve the Nigerian indigenous people and their built environments. While the study provides an empirical base for data-based policy, planning, and implementation of needed developments in the area in context, there is a need to explore individual constructs further to confirm the reliability of the

results. Practically applied studies on each attribute, consequence, and value should be further conducted to develop concrete scientific and technological strategies for transformative improvements.

References

Achoba, M. I., Majid, R. B. A. & Obiefuna, C. O. (2021). Relationship between window and view factors in the workplace: a SEM approach. International Journal of Built Environment and Sustainability, 8 (2), 103–113. https://doi.org/10.11113/ijbes.v8.n2.667

Aule, T. T., Jusan, M. B. M. & Ayoosu, M. I. (2019). Outcomes of community participation in housing development: an update review. International Journal of Scientific Research in Science, Engineering and Technology, 6 (6), 208–218. https://doi.org/10.32628/ijsrset196642

Aule, T. T., Majid, R. B. A., Jusan, M. B. M. & Ayoosu, M. I. (2022). Exploring motivational factors of indigenous house form for value-based development: the Tiv people of central Nigeria in context. International Journal of Sustainable Development and Planning, 17 (2), 683–691. https://doi.org/10.18280/ijsdp.170234

Car-Pušić, D., Tijanić, K., Marović, I. & Mladen, M. (2020). Predicting buildings construction cost overruns on the basis of cost overruns structure. Scientific Review Engineering and Environmental Sciences, 29 (3), 366––376. https://doi.org/10.22630/PNIKS.2020.29.3.31

Ezennia, I. S. & Hoskara, S. O. (2021). Assessing the subjective perception of urban households on the criteria representing sustainable housing affordability. Scientific African, 13, e00847. https://doi.org/10.1016/j.sciaf.2021.e00847

Gaskin, J., James, M. & Lim, J. (2019). Master validity too: AMOS Plugin. Retrieved from: http://statwiki.gaskination.com

Isah, A. D. & Khan, T. H. (2016). Re-emergence of indigeneity in transformed layouts in urban public housing in Nigeria. International Journal of Built Environment and Sustainability, 3 (1), 1–9. https://doi.org/10.11113/ijbes.v3.n1.104

Kline, R. B. (2016). Principles and practices of structural equation modelling. New York: The Guilford Press.

Maina, J. J. (2013). Uncomfortable prototypes: Rethinking socio-cultural factors for the design of public housing in Billiri, north east Nigeria. Frontiers of Architectural Research, 2 (3), 310–321. https://doi.org/10.1016/j.foar.2013.04.004

Malhotra, N. K. (2020). Marketing research: an applied orientation. Harlow: Pearson Education.

Neef, A., Benge, L., Boruff, B., Pauli, N., Weber, E. & Varea, R. (2018). Climate adaptation strategies in Fiji: The role of social norms and cultural values. World Development, 107, 125–137. https://doi.org/10.1016/j.worlddev.2018.02.029

Ostańska, A. (2019). Monitoring the resident's needs: Input for the pre-construction stage of rehabilitation projects in housing estates. Scientific Review Engineering and Environmental Sciences, 28 (3), 383–393. https://doi.org/10.22630/PNIKS.2019.28.3.36

Pahlevan Sharif, S. & Sharif Nia, H. (2018). Structural equation modeling with AMOS. Tehran: Artin Teb.

Sharif, S. P., Mostafiz, I. & Guptan, V. (2018). A systematic review of structural equation modelling in nursing research. Nurse Researcher, 26 (2), 28–31. https://doi.org/10.7748/nr.2018.e1577

Umar, G. K., Yusuf, D. A., Ahmed, A. & Usman, A. M. (2019). The practice of Hausa traditional architecture: Towards conservation and restoration of spatial morphology and techniques. Scientific African, 5, e00142. https://doi.org/10.1016/j.sciaf.2019.e00142

UN General Assembly (2016). Preparatory committee for the united nations conference on housing and sustainable urban development (Habitat III). Policy Paper 10: Housing Policies. New York: United Nations.

United Nations SDGs (2015). Transforming our world: The 2030 Agenda for Sustainable Development. Retrieved from: http://www.un.org/en/development/desa/news/sustainable/un-adopts-new-global-goals.html#more-15178

Wang, J., Zhao, J. L., Wu, T. Y. & Tang, L. K. (2017). New-type intensive rural settlements in China based on the unified and self-construction mechanisms of spatial organization. International Journal of Sustainable Development and Planning, 12 (6), 1073–1084. https://doi.org/10.2495/SDP-V12-N6-1073-1084

Summary

Exploring cultural values and sustainability preferences in housing development: A structural equation modeling approach. The study aimed to establish the relationship between values and people's preferences for sustainable improvement in Nigeria's indigenous housing context. The relationship was tested in SEM using ordinal survey data obtained between February and March 2022 with 241 valid samples. The mainstream values were statistically validated using CFA while the relationships were generated in the SEM. Results established a significant relationship between values and the people's preferences for transformative improvements. The findings provide a foundation for long-term policy formation, practical transformative experimentation, and an empirical foundation for future methodological research.

Scientific Review Engineering and Environmental Sciences (2022), 31 (3), 161–175

Sci. Rev. Eng. Env. Sci. (2022), 31 (3) https://srees.sggw.edu.pl

ISSN 1732-9353 (suspended) eISSN 2543-7496 DOI 10.22630/srees.3150

Received: 13.06.2022
Accepted: 21.07.2022

Atheer S. ISSA✉ https://orcid.org/0000-0002-8702-2952

Ali K. Al-ASADI

University of Thi-Qar, College of Engineering, Civil Engineering Department, Iraq

MECHANICAL PROPERTIES OF LIGHTWEIGHT EXPANDED CLAY AGGREGATE (LECA) CONCRETE

Key words: lightweight concrete, mechanical properties, lightweight expanded clay aggregate, LECA concrete

Introduction

The self-weight of concrete construction accounts for a major amount of the total load on the structure. Therefore, decreasing the density of concrete has obvious advantages. Lightweight concrete (LWC) has become one of the most essential materials in construction today, because of its practical and economic advantages (American Concrete Institute [ACI], 2014b). The self-weight of normal concrete is about 2,400–2,500 kg·m^{-3}, this makes it very heavy, and the size of structural members increases as a result of the overall dead load. The LWC is a form of concrete that contains either lightweight aggregate (LWA) or an expanding agent. The dry density of LWC ranges from 300 to 1,840 kg·m^{-3}, and it weighs 23–80% less than conventional weight concrete. When compared to conventional weight concrete, which has a unit weight of 2,400 kg·m^{-3}, the unit weight of LWC for structural usage ranged between 1,400 and 2,000 kg·m^{-3} (Agrawal, Gupta, Sharma, Panwar & Siddique, 2021). Lightweight aggregate has many advantages when used in producing the concrete such as reducing a dead load of a structure elements that may result in reduced foundation size and large area availability due to reduction in the dimensions size of columns, slabs, and beams, high thermal and sound insulation, enhanced fire resistance (El-Sayed, Heniegal, Ali & Abdelsalam, 2013). For structural LWC applications, the 28-day compressive strength should be greater than 17 MPa (Abdulrazzaq & Khadhim, 2019; Ahmad, Chen & Shah, 2019). Nowadays, many types of LWA can be utilized to make lightweight concrete such as expanded

✉Enga92th@utq.edu.iq

Issa, A. S., Al-Asadi, A. K. (2022). Mechanical properties of lightweight expanded clay aggregate (LECA) concrete. *Sci. Rev. Eng. Env. Sci.*, *31* (3), 161–175. DOI 10.22630/srees.3150

clays, slate, shale, pumice, etc. (Agrawal et al., 2021). One of the LWA types that are utilized in structure construction is light expanded clay aggregate (LECA), which is a kind of artificially produced LWA that is created by expanding the natural clay at a high temperature of around 1,200°C (2,190°F) in a horizontal rotary kiln. Thousands of tiny bubbles are formed during the heating process, expands the clay about 5–6 times about its original volume, forming a honeycomb structure. The LECA has a spherical or potato shape appearance because of the circular movement in the kiln with they have a secured and barely porous external surface as compared to internal structure that is black in the color and highly porous (Ahmad et al., 2019). For the production of LWC, the use of increasing amounts of cement becomes even more important. However, increasing the cement content for constant water content has generally improved the workability of these mixes, allowing for lower w/c ratios. Water content is reduced by using a superplasticizer. The use of a higher cement content paired with a lower w/c ratio may have contributed to the improved quality of the LWC matrix. Silica fume has risen in popularity in recent years as a result of its high reactivity potential, which is boosted by its large specific surface area. It works as a pozzolan when it reacts with the lime that is released during the hydration of Portland cement. There needs to be a lot of research done on the role of silica fume as well as the effects of aggregate on mechanical properties and durability (Mahdy, 2016). Dilli, Atahan and Şengül (2015) worked on different mixes of LWC using LECA with different unit weights 1,640 and 2,050 $kg \cdot m^{-3}$ to investigate the compressive strength, modulus of elasticity (MOE), Poisson's ratio, and the ductility of LWC to compare them with mixes of normal concrete (NC). The results showed that the compressive strength of LWC mixtures varied between 20 and 70 MPa. As well, LWC mixtures changed significantly in terms of elastic properties and ductility compared with NC mixtures. When compared to NC mixes, LWC mixtures showed a significant decrease in MOE and more brittle behavior throughout the same compressive strength range. Sonia et al. (2016) studied the properties of lightweight aggregate concrete (LWAC) using LECA as coarse aggregate with different ratios such as 20, 40, 60, 80, and 100% and compared them with NWC using fly ash ratios such as 15, 20 and 25% as a partial substitute for cement in concrete. The LWAC has shown a reduction in compressive strength and split tensile strength from 34.60–21.77 and 3.20–1.57 MPa, respectively, with an increase in LECA content from 0 to 100%. The values obtained for the LECA concrete when substituted with 40 and 60% of coarse aggregate showed better results when compared to NWC. Similarly, they found out that the replacement of cement with 15% fly ash gives better results. With various mix proportions, the use of fly ash and LECA, at 15 and 40%, shows higher compressive strength and tensile strength and thus can be recommended for structural purposes. Patel, Shah and Desai (2019) investigated the effect of partially replacing coarse aggregate with (LECA) on concrete mechanical properties. The percentage of replacement of normal aggregate ranges from 0–100% with an increment of 25%. The results show that the compressive strength decreased as the LECA content increased. The compressive strength, split tensile strength, and flexural strength

decreased by 16.87, 17.20, and 13.29%, respectively, after 28 days of curing, along with a reduction in weight of about 28% with 100% LECA replacement of normal aggregate. Nevertheless, with 25% LECA replacement, negligible loss of strength is noted. To improve the mechanical properties of concrete containing LECA, materials such as silica fume, fly ash, slag, steel fiber, and polypropylene fiber can be used to increase its strength.

The aim of this work is to present an experimental study of the mechanical properties of LECA concrete. An effort was made in this study to examine the impact of adding silica fume (SF) to the structural LWC as an attempt to enhance strength performance. It's commonly used in concrete constructions that demand high strength or low water permeability as a partial replacement for cement. It is also known to be very reactive. Because of this, it is used in small amounts to improve the microstructure of concrete. The percentage of replacement of LECA (100%) instead of coarse aggregate. In addition, two kinds of concrete admixtures were used in this research; silica fume with a percentage of 8% of cement weight and superplasticizer with a percentage of 0.95% of cementitious materials (cement and silica fume).

Material properties

The materials used in this study are: Portland cement, fine aggregate (sand), light expanded clay aggregate (LECA) as a full replacement for the coarse aggregate, silica fume, superplasticizer.

Cement

Portland cement was utilized in the current study. Tables 1 and 2 show the chemical and physical properties of Portland cement, respectively. The properties of cement meet the requirements of ASTM C150/C150M-21 (ASTM International [ASTM], 2021).

Fine aggregate

The available natural fine aggregate (sand) that has a maximum size of 4.75 mm was used for the LWC mixture. The test

TABLE 1. Chemical properties of cement

Chemical properties	SiO_2	CaO	MgO	Fe_2O_3	Al_2O_3	SO_3	Loss on ignition	Insoluble residue	Lime saturated factor	C_3A
Tested cement [%]	21.67	57.3	2.83	3.8	3.5	2.25	3.9	1.42	0.83	2.9
ASTM C150/C150M-21	–	–	≤ 5	–	–	≤ 2.8	≤ 4	≤ 1.5	0.66–1.02	≤ 5

TABLE 2. Physical properties of cement

Physical properties	Tested cement	ASTM C150/C150M-21
Vicat initial time of setting [min]	156	not less than 45 min
Vicat final time of setting [min]	226	not more than 375 min
Average compressive strength, age (3 days) [MPa]	18.9	≥ 8
Average compressive strength, age (7 days) [MPa]	23.8	≥ 15

Issa, A. S., Al-Asadi, A. K. (2022). Mechanical properties of lightweight expanded clay aggregate (LECA) concrete. *Sci. Rev. Eng. Env. Sci.*, *31* (3), 161–175. DOI 10.22630/srees.3150

TABLE 3. Sand gradation and sulphate content

Specification	Sieve size [mm]							Pan	Sulphate
	9.5	4.75	2.36	1.18	0.6	0.3	0.15		
Cumulative passing [%]	100	98	90	77	56	20	1	–	0.4
Passing [%] (acc. ASTM C33/C33M-13)	100	90–100	80–100	50–85	25–60	5–30	0–10	–	< 0.5

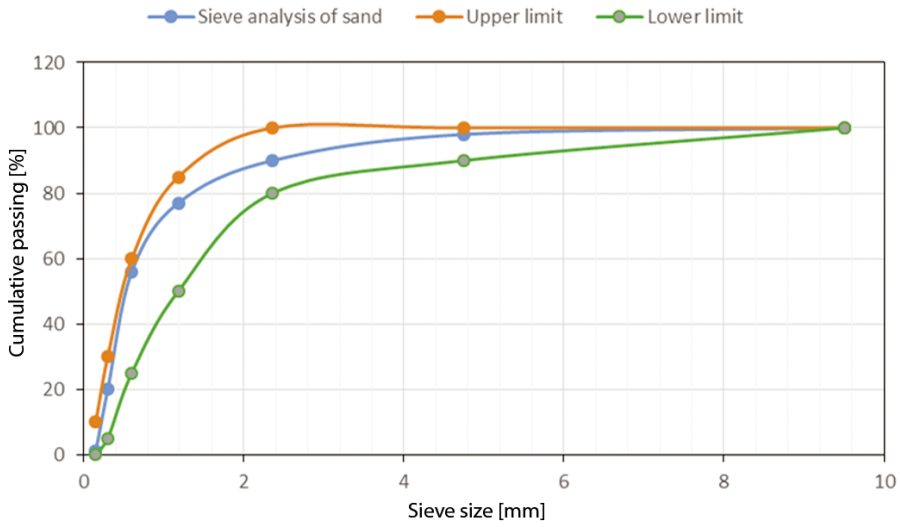

FIGURE 1. Sieve analysis of fine aggregate

results meet the requirements of ASTM C33/C33M-13 (ASTM, 2013a). The sand gradation and sulphate are presented in Table 3 and Figure 1.

Lightweight expanded clay aggregate (LECA)

The LECA was used in this study at a maximum size of 10 mm as a lightweight aggregate in all LWC mixtures. In this study, expanded clay aggregate, as shown in Figure 2, was used as a full replacement for the coarse aggregate. The test results meet the requirements of ASTM C330/ /C330M-17A (ASTM, 2017). The gradation

FIGURE 2. Shows lightweight expanded clay aggregate (LECA) used in the current study

TABLE 4. Lightweight expanded clay aggregate (LECA) gradation results

Specification	Sieve size [mm]				
	12.5	9.5	4.75	2.36	1.18
Cumulative passing [%]	100	88	9	3	1
Passing [%] (acc. ASTM C330/C330M-17A)	100	80–100	5–40	0–20	0–10

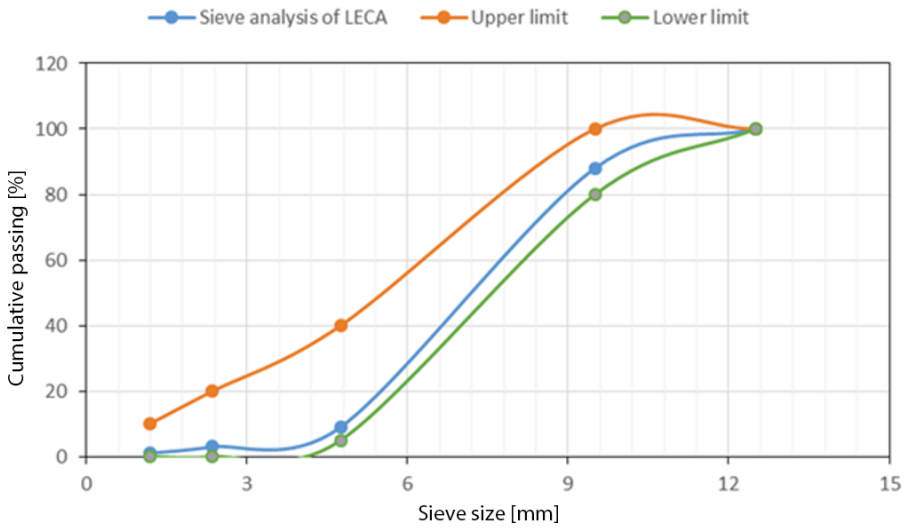

FIGURE 3. Sieve analysis of lightweight expanded clay aggregate (LECA)

TABLE 5. Physical properties of lightweight expanded clay aggregate (LECA)

Physical properties	Dry density [kg·m^{-3}]	Absorption [%]	Specific gravity	Maximum size [mm]
Value	415	20	0.62	10

and physical properties of test results of LECA are listed in Table 4 with Figure 3 and Table 5, respectively.

Silica fume (SF)

Silica fume is a very fine pozzolanic material produced in electric arc furnaces for silicon or alloys containing silicon, with particles around 100 times less than an average cement grain (Holland, 2005). Silica fume was used in this study with three values (4, 8 and 12%) as a partial replacement of cement weight to choose the best ratio to be added to the LWC mixture. Figure 4 shows the type of SF used. Tables 6 and 7 show the physical and chemical characteristics of SF, respectively, according to the manufacturers specifications, which conform to ASTM C1240-05 requirements (ASTM, 2005).

Issa, A. S., Al-Asadi, A. K. (2022). Mechanical properties of lightweight expanded clay aggregate (LECA) concrete. *Sci. Rev. Eng. Env. Sci.*, *31* (3), 161–175. DOI 10.22630/srees.3150

FIGURE 4. Sample of silica fume used in the current study

TABLE 6. Physical characteristics of silica fume (SF)

Physical characteristics	Tested SF	ASTM C1240-05 requirements
Max, % percentage retained on a 45 m (No 325) sieve	2	< 10
Index of accelerated pozzolanic strength activity	105	< 105
Specific surface [$m^2 \cdot g^{-1}$]	24	< 15

TABLE 7. Chemical characteristics of silica fume (SF)

Chemical characteristics	SiO_2	CaO	SO_3	Cl	Loss on ignition
Tested cement [%]	90	0.8	0.2	0.035	4
ASTM C1240-05	≥ 85	–	–	–	≤ 6

Superplasticizer (SP)

In this study, the Sika Visco Crete 5930 IQ with a ratio of 0.95% of cement weight was used, which meets the specification described in ASTM C494/C494M-19 (ASTM, 2019). The SP is also called high range water--reducing admixtures (HRWRA). This type of SP reduces the quantity of water while improving the workability and working to prevent the segregation issue. The properties of this type are shown in Table 8 according to the manufacturer's specifications.

Water

Potable water was used throughout the experimental work necessary to produce the concrete mixes, while tap water provided in the university site was used in curing all specimens.

Mix design

Structural lightweight aggregate concrete has a density of less than 2,000 $kg \cdot m^{-3}$ and a cylinder compressive strength of greater than 17 MPa at 28 days. According to previous researches, and based on ACI 211.2-04 (ACI, 2004), which is used as a design guide for lightweight concrete mixtures, many trial mixes were made to select the proportion of the mixture ingredients that satisfied the required compressive strength and density for lightweight concrete. Because of the LECA's high water absorption capacity, more water was added (approximately 20% of the LECA weight over the amount of water used in the control mix) to keep the slump within the 20–100 mm range. In order to ensure the adequacy of the trial

TABLE 8. Properties of superplasticizer

Property	Specific gravity	Chloride content	Appearance	Recommended dosage	Storage life
Description	1.085	nil	turbid liquid	0.8–2% by weight of binder for flowing concrete	up to 1 year in closed containers

mixtures for the compressive strength, three concrete cubes with a dimension of 150 × 150 × 150 mm were cast for each trial mix. After 24 h, concrete cubes were demold and then cured at ambient temperature for 7 days. After 7 days of curing, concrete cubes were left to dry in fresh air for 4 h prior to the concrete compressive strength test. A digital compression machine with a maximum capacity of 2,000 kN was used to test the concrete cube's compressive strength at the Civil Engineering Structural Laboratory at the University of Thi-Qar in Iraq. Mix proportion (by weight), slump, weight of specimen, hardened density, and compressive strength of the trail mixes are illustrated in Table 9. Figure 5 shows some trial mixes and their compression tests.

TABLE 9. Trial mixes proportions

Trail mix (T.M)	T.M (1)	T.M (2)	T.M (3)	T.M (4)	T.M (5) selected	T.M (6)
Cement [kg·m^{-3}]	500	500	500	480	460	440
Silica fume [%]	–	4	–	4	8	12
Fine aggregate [kg·m^{-3}]	872	872	936	936	936	936
Lightweight expanded clay aggregate [kg·m^{-3}]	230	230	180	180	180	180
Superplasticizer [%]	0.8	0.8	0.95	0.95	0.95	0.95
Water [kg·m^{-3}]	180	187	190	190	190	190
w/c or b/c	0.36	0.36	0.38	0.38	0.38	0.38
Slump [mm]	33	30	80	90	90	90
Weight of specimen [g]	5 933	5 924	6 168	6 149	6 152	6 155
Cube compressive strength [MPa]	18	20	23	25	27.8	30.5
Density [kg·m^{-3}]	1 760	1 757	1 833	1 828	1 821	1 824

FIGURE 5. Some trial mixes and their compression tests

Issa, A. S., Al-Asadi, A. K. (2022). Mechanical properties of lightweight expanded clay aggregate (LECA) concrete. *Sci. Rev. Eng. Env. Sci.*, *31* (3), 161–175. DOI 10.22630/srees.3150

Casting of LWC test specimens

Steel cubes with standard dimensions of 150 × 150 × 150 mm were used in the current study to cast the concrete cube specimens to determine the concrete compressive strength of the LWC specimens. In addition, steel cylinders with dimensions of 150 × 300 mm (diameter × height) were used to cast and test concrete cylinders for indirect splitting tensile strength and to draw a stress–strain relationship. As well, steel prisms with standard dimensions of 100 × 100 × 500 mm were used to determine the modulus of rupture of LWC. Table 10 presents the mixing proportions from the trail mixes for the casting of the test specimens in the presence of an admixture, which meets the specifications of ASTM C494/C494M-19 – Type F (ASTM, 2019). According to BS 1881-116 (BSI, 1991), a cube compressive design strength of 30 MPa was specified for the reference concrete mix. In general, six cubes, three cylinders, and three prisms were cast. To avoid moisture loss, all specimens (concrete cubes, cylinders, and prisms) were covered with plastic bags. All specimens were kept moist for 36 h, after which the formwork was stripped and cured under identical conditions for 28 days.

TABLE 10. Lightweight concrete (LWC) mix proportions

Mix type	Cement [kg·m^{-3}]	Silica fume [kg·m^{-3}]	Light expanded clay aggregate [kg·m^{-3}]	Fine aggregates [kg·m^{-3}]	Superplasticizer [kg·m^{-3}]	Water [kg·m^{-3}]
LWC	460	40	180	936	4.75	190

Testing methods

Test of fresh concrete (slump test)

The workability of the LWC mix was checked immediately after mixing using the slump test, as stated in ASTM C143/C143M-15 (ASTM, 2015b). The procedure of the test consists of filling the concrete to the slump cone in three equivalent layers. Each layer is tamped with a tamping rod about 25 times. The excess concrete is removed from the top edge of the cone by the tamping rod. The cone is raised vertically and quickly and the amount is measured by the slumps of the concrete sample. The slump value is gotten from the distance between the highest point on the surface of the slumped concrete sample and the underside of the round tamping bar. The slump value was 90 mm. The type of slump is recorded as a "true slump", as shown in Figure 6.

Mechanical properties of the hardened samples of LWC

At the age of 28 days, each sample of hardened concrete contains five main properties. These properties are compressive strength (f_{cu}), splitting tensile strength (f_{ct}), modulus of rupture (f_r), static modulus of elasticity (E_c), and density (D).

Compressive strength (f_{cu})

The compressive strength of hardened concrete is performed after 7 and 28 days of curing, in accordance with BS 1881-116 (BSI, 1991) using a digital compression

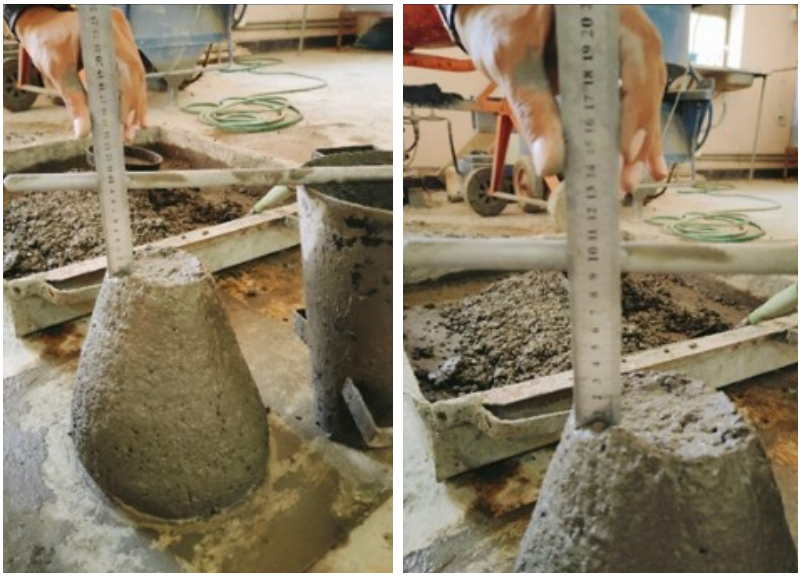

FIGURE 6. Slump test

machine with a capacity of 2,000 kN, as illustrated in Figure 7a. Cubes of 150 × 150 × 150 mm were used to determine the concrete's compressive strength. The tests were conducted at ages 7 and 28 days, and three specimens were tested at each age. The specimen is aligned carefully at the center of thrust of the higher bearing block and loading is applied continuously until failure. The average value of three specimens was taken; it is 28 MPa at age 7 days and 32 MPa at age 28 days. Figure 7b illustrates the compressive strength test failure shape.

Splitting tensile strength (f_{ct})

The splitting tensile strength (indirect tensile strength) tests are executed on three cylindrical samples of LWC in accordance with ASTM C496/C496M-11

FIGURE 7. Compressive strength test: a – testing machine; b – the cubes after failure

Issa, A. S., Al-Asadi, A. K. (2022). Mechanical properties of lightweight expanded clay aggregate (LECA) concrete. *Sci. Rev. Eng. Env. Sci.*, *31* (3), 161–175. DOI 10.22630/srees.3150

(ASTM, 2004). The splitting-tension test calculates the concrete tensile strength. In this test, a concrete cylinder (150 × × 300 mm) is exposed to a compressive loading along the vertical diameter till failure by using a thin strip of plywood which is placed between the sample and the upper bearing blocks of the testing machine. The average value of three cylinders is considered, according to the equation:

$$f_{ct} = \frac{2P}{\pi DL}, \tag{1}$$

where:
f_{ct} – splitting tensile strength [MPa],
P – load up on failure [N],
D – cylinder's diameter [mm],
L – cylinder's length [mm].

Table 11 presents the splitting tensile strength test results for LWC samples and the values obtained by the equation of ACI 318M-14 (ACI, 2014a) equal to $\lambda 0.56\sqrt{f'_c}$ MPa (where λ symbolize reduction factor equals 0.85 for LWC, and f'_c means cylinder compressive strength measured in MPa), which showed good agreement with the test results. Figure 8 shows the stages of test and mode of failure for LWC samples.

TABLE 11. Splitting tensile strength of tested lightweight concrete (LWC) specimens

Tested sample	Measuring f_{ct} [MPa]	Predicted f_{ct} [MPa]
LWC	2.95	2.26

Modulus of rupture (f_r)

The LWC samples are subjected to flexural strength (modulus of rupture) tests in accordance with ASTM C78/C78M--15A (ASTM, 2015a). The flexural strength tests are performed on three prism samples 100 × 100 × 500 mm with four points of loading, as shown in Figure 9. A comparison between the theoretical values determined by ACI 318M-14 (ACI, 2014a) equal to $\lambda 0.62\sqrt{f'_c}$ MPa and the experimental results of modulus of rupture is presented in Table 12. The estimation of flexural strength is given in the following equation:

$$f_r = \frac{PL}{bd^2}, \tag{2}$$

where:
f_r – modulus of rupture [MPa],
P – maximum applied load (failure load) [N],
L – distance between the center of one support to the center of the other [mm],
b – prism width [mm],
d – prism depth [mm].

FIGURE 8. Splitting tensile test

TABLE 12. Flexural strength value (f_r) of tested lightweight concrete (LWC) specimens

Tested sample	Measuring f_r [MPa]	Predicted f_r [MPa]
LWC	3.66	2.50

Static modulus of elasticity of LWC (E_c)

This test technique offers a ratio of stress to strain value for standard hardened concrete cylindrical specimens. The modulus of elasticity is the degree of resistance of the material to deformation. The modulus of elasticity for lightweight strength is measured according to ASTM C469/C469M-10 (ASTM, 2010) using three cylindrical specimens with dimensions 150 × 300 mm, tested in the laboratory under the uniaxial compression load. An average of three cylinders was used. The following expression is used to compute the static modulus of elasticity:

$$E_c = \frac{(S_2 - S_1)}{(\varepsilon_2 - 0.00005)}, \quad (3)$$

where:
E_c – static modulus of elasticity [MPa],
S_2 – stress corresponds to 40% of ultimate load [MPa],
S_1 – stress corresponds to longitudinal strain (0.00005) [MPa],
ε_2 – longitudinal strain induced by the stress S_2.

TABLE 13. Static modulus of elasticity (E_c) value of tested lightweight concrete (LWC) specimens

Tested sample	Measuring E_c [MPa]	Predicted E_c [MPa]
LWC	12 506	15 893

FIGURE 9. Set-up of modulus of rupture test

FIGURE 10. Modulus of elasticity test and mode of failure for samples

Issa, A. S., Al-Asadi, A. K. (2022). Mechanical properties of lightweight expanded clay aggregate (LECA) concrete. *Sci. Rev. Eng. Env. Sci.*, *31* (3), 161–175. DOI 10.22630/srees.3150

Table 13 presents the static modulus of elasticity from test results for LWC samples and the values obtained by the equation of ACI 318M-14 (ACI, 2014) equal to $0.043(W_c)^{1.5}\sqrt{f_c'}$ MPa (where W_c symbolize unit weight measured in kg·m^{-3}). Figure 10 shows the stages of test and mode of failure for LWC samples. In addition, cone and split-type failures occurred in the LWC cylinders, as shown in Figure 10.

Density (D)

Density was calculated using three (150 mm) cubes on average, as specified by ASTM C642-13 (ASTM, 2013b), and the result was 1,823 kg·m^{-3}. The density of the specimen was determined by weighing it after modelling and drying. The following equation can be used to find the density of the specimen:

$$D = \frac{M}{V}, \tag{4}$$

where:
D – density [kg·m^{-3}],
M – weight of specimen [kg],
V – volume [m^3].

Results and discussion

Hardened LWC samples' mechanical properties

The mechanical properties of LWC (compressive strength, flexural strength, splitting tensile strength, density, and modu-lus of elasticity) were tested after 28 days; the results are listed in Table 14. The cubes, cylinders, and prisms were used in dimensions of 150 × 150 × 150, 150 × 150 × 300, and 100 × 100 × 500 mm, respectively. An average of three specimens is considered for the mix. The results show that the ratio of strength-to-density or strength-to-weight is efficient in structural elements. The strength capacity can generally be increased by reducing the maximum size of the coarse aggregate. The LWC in this work uses LECA as coarse aggregate. According to ASTM C330/C330M-17A (ASTM, 2017), structural lightweight aggregate concrete must have a splitting tensile strength of 2 MPa or higher. From the test, the LECA concrete is 47% more than the minimum requirement of ASTM C330/C330M-17A. The LECA concrete has a splitting tensile to compressive strength ratio of around 13%. A decreased flexural/ /compressive strength ratio was also observed for the LWC in comparison to the normal weight concrete (NWC).

Stress–strain curve

Figure 11 shows the stress–strain curve for the LWC specimen. The modulus of elasticity of concrete is based on the modulus of each component and how they are mixed together. The NWC has a higher modulus of elasticity than the LWC because the moduli of sand, stone, and gravel are greater than the moduli of lightweight constituents. Several expressions for the modulus of elasticity of concrete have been developed over the years.

TABLE 14. Mechanical properties of tested lightweight concrete (LWC) specimens

Tested sample	f_{cu} [MPa]	$f'c$ [MPa]	$\frac{f'c}{f_{cu}}$	f_{sp} [MPa]	f_r [MPa]	Density (d) [kg·m^{-3}]	E_c [MPa]
LWC	32	22.55	0.7	2.95	3.66	1 823	12 506

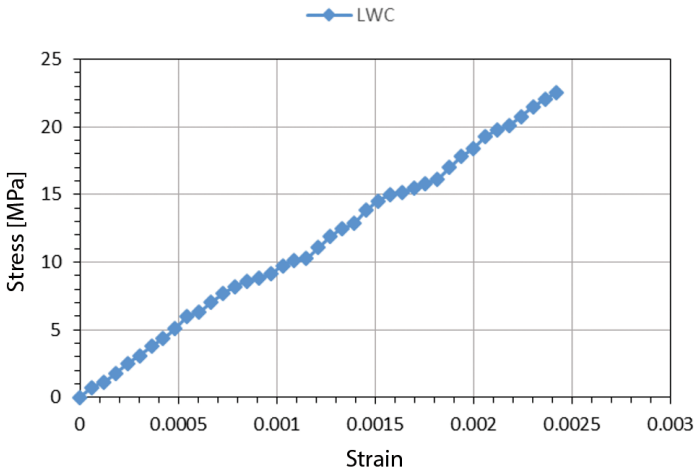

FIGURE 11. Experimental stress–strain curve for lightweight concrete (LWC)

However, the increased use of lightweight and higher-strength concrete has led to a need for a more precise expression. The results demonstrate a 27% variation in the modulus of elasticity between the calculated and tested values. It is clear from the figure that the stress–strain curve exhibits more extended linear and elastic behavior. Furthermore, the strain at failure is approximately 0.0024 for LWC. In addition, a cone and split failure mode occurred in the cylinders of LWC, as shown in Figure 10.

Conclusions

Based on the findings acquired from the laboratory tests performed in this study, it can be inferred that the concrete produced can be categorized as LWC. In the case of LECA, it has been discovered that it is ideal for usage in structural elements due to its qualities, which include being lightweight and having sufficient strength when compared to other lightweight aggregates. This type of LWC, with a compressive strength of 32 MPa and a density of 1,823 kg·m^{-3}, could be used in the structural and non-structural elements. The results show that the reduction in the strength of LWAC was found to be higher in the concrete with an estimated compressive strength of 32 MPa due to the lower strength of the LWA (expanded clay). The mechanical properties of LWC are significantly improved by adding SF by improving the microstructure of the concrete. In comparison to ASTM C33/C33M-13 (ASTM, 2013a), LECA concrete has a splitting tensile strength that is 47% higher. The LECA concrete has a splitting tensile to compressive strength ratio of around 13%. A decreased flexural/compressive strength ratio was also observed for the LWC.

References

Abdulrazzaq, O. A. & Khadhim, A. M. (2019). Studying the behaviour of lightweight deep beams with openings. *International Journal of Engineering Technologies and Management Research*, *6* (12), 89–100. https://doi.org/10.29121/ijetmr.v6.i12.2019.558

Agrawal, Y., Gupta, T., Sharma, R., Panwar, N. L. & Siddique, S. (2021). A comprehensive review on the performance of structural lightweight aggregate concrete for sustainable construction. *Construction Materials*, *1* (1), 39–62. https://doi.org/10.3390/constrmater1010003

Ahmad, M. R., Chen, B. & Shah, S. F. A. (2019). Investigate the influence of expanded clay aggregate and silica fume on the properties of lightweight concrete. *Construction and Building Materials*, *220*, 253–266. https://doi.org/10.1016/j.conbuildmat.2019.05.171

American Concrete Institute [ACI] (2004). *Standard Practice for Selecting Proportions for Structural Lightweight Concrete* (ACI 211.2-04). Farmington Hills, MI: American Concrete Institute.

American Concrete Institute [ACI] (2014a). *Building Code Requirements for Structural Concrete and Commentary* (ACI 318M-14). Farmington Hills, MI: American Concrete Institute.

American Concrete Institute [ACI] (2014b). *Guide for structural lightweight-aggregate concrete* (ACI 213R-14). Farmington Hills, MI: American Concrete Institute.

ASTM International [ASTM] (2005). *Standard specification for silica fume used in cementitious mixtures* (ASTM C1240-05). West Conshohocken, PA: ASTM International.

ASTM International [ASTM] (2010). *Standard test method for static modulus of elasticity and Poisson's ratio of concrete in compression* (ASTM C469/C469M-10). West Conshohocken, PA: ASTM International.

ASTM International [ASTM] (2011). *Standard test method for splitting tensile strength of cylindrical concrete specimens* (ASTM C496/C496M-11). West Conshohocken, PA: ASTM International.

ASTM International [ASTM] (2013a). *Standard Specification for Concrete Aggregates* (ASTM C33/C33M-13). West Conshohocken, PA: ASTM International.

ASTM International [ASTM] (2013b). *Standard Test Method for Density, Absorption, and Voids in Hardened Concrete* (ASTM C642--13). West Conshohocken, PA: ASTM International.

ASTM International [ASTM] (2015a). *Standard Test Method for Flexural Strength of Concrete (Using Simple Beam with Two-Point Loading)* (ASTM C78/C78M-15A). West Conshohocken, PA: ASTM International.

ASTM International [ASTM] (2015b). *Standard Test Method for Slump of Hydraulic-Cement Concrete* (ASTM C143/C143M-15). West Conshohocken, PA: ASTM International.

ASTM International [ASTM] (2017). *Standard specification for lightweight aggregates for structural concrete* (ASTM C330/C330M-17A). West Conshohocken, PA: ASTM International.

ASTM International [ASTM] (2019). *Standard Specification for Chemical Admixtures for Concrete* (ASTM C494/C494M-19). West Conshohocken, PA: ASTM International.

ASTM International [ASTM] (2021). *Standard Specification for Portland Cement* (ASTM C150/C150M-21). West Conshohocken, PA: ASTM International.

British Standards Institution [BSI] (1991). *Testing Concrete. Part 116: Method for Determination of Compressive Strength of Concrete Cubes* (BS 1881-116). London: British Standards Institution.

Dilli, M. E., Atahan, H. N. & Şengül, C. (2015). A comparison of strength and elastic properties between conventional and lightweight structural concretes designed with expanded clay aggregates. *Construction and Building Materials*, *101*, 260–267.

El-Sayed, W. S., Heniegal, A. M., Ali, E. E. & Abdelsalam, B. A. (2013). Performance of lightweight concrete beams strengthened with GFRP. *Port Said Engineering Research Journal*, *17* (2), 105–117.

Holland, T. C. (2005). *Silica fume – User's manual*. Washington DC: Federal Highway Administration, Silica Fume Association (SFA).

Mahdy, M. (2016). Structural lightweight concrete using cured LECA. *International Journal of Engineering and Innovative Technology*, *5* (9), 25–31.

Patel, K. R., Shah, S. G., Desai, K. (2019). To Study the Effect of Addition of Lightweight Expanded Clay Aggregate on fresh and hardened properties of Concrete. *International Journal of Technical Innovation in Modern Engineering & Science*, *5* (4), 126–131.

Sonia, T. & Subashini, R. (2016). Experimental Investigation on Mechanical Properties of Light Weight Concrete Using Leca. *International Journal of Science and Research*, *5* (11), 1511–1514.

Summary

Mechanical properties of lightweight expanded clay aggregate (LECA) concrete. The construction activities are based on structural concrete, which is one of the most commonly used materials. The fundamental aim of using lightweight concrete (LWC) was to reduce the concrete self-weight of the structure parts. As a result, LWC has been used successfully in a variety of installations for several years. In this paper, the mechanical properties of concrete made with lightweight expanded clay aggregate (LECA) as a full replacement for coarse aggregate are studied. The experimental program shows that LECA with a 32 MPa cube compressive strength and an 1,823 kg·m^{-3} dry density can be used to make structural lightweight aggregate concrete (SLWC). The results show that the reduction in the strength of lightweight aggregate concrete (LWAC) was found to be higher in the concrete with an estimated compressive strength of 32 MPa due to the lower strength of the LWA (expanded clay). According to the test results, the mechanical properties of LWC were greatly improved by adding silica fume (SF). Furthermore, LECA concrete has a splitting tensile strength that is 47% higher than the ASTM C330/C330M-17A minimum requirement. The LECA concrete has a splitting tensile strength to compressive strength ratio of approximately 13%. Additionally, the results demonstrate a 27% difference in the modulus of elasticity between the calculated and tested values.

Scientific Review Engineering and Environmental Sciences (2022), 31 (3), 176–189

Sci. Rev. Eng. Env. Sci. (2022), 31 (3) https://srees.sggw.edu.pl

ISSN 1732-9353 (suspended) eISSN 2543-7496 DOI 10.22630/srees.3373

Received: 24.07.2022
Accepted: 29.09.2022

Hassan Al-MOUSAWEY✉

Basim Sh. ABED

University of Baghdad, Collage of Engineering, Baghdad, Iraq

SIMULATION AND ASSESSMENT OF WATER SUPPLY NETWORK FOR AL-NASIR NETWORK AT AL-NAJAF GOVERNORATE

Key words: hydraulic analysis, WaterGEMS, water distribution network, residual chlorine

Introduction

Water is one of the basic necessities for healthy existence. Having a sufficient supply of drinkable water promotes both the welfare of the population and the best possible growth of many industries (Albadry, 2017; Ho, Puika & Kasih, 2020). The inefficient everyday functioning of a water distribution system (WDS) imposes considerable consequences even if failure occurrences are unavoidable and frequently spectacular and expensive. Performance measurement is essential in engineering the operation and management of any WDS (Hussein, 2021). Modelling WDS is used to acquire an accurate idea of the network's operation and to identify the causes and situations that influence the network's performance (van Summeren & Blokker, 2017).

Managing the amount of free residual chlorine in water distribution systems is crucial for ensuring that end-user tap water is safe for consumption. Residual chlorine level should be between 0.2 and 0.5 $mg \cdot L^{-1}$ to eliminate pathogens without causing bad taste (Alsaydalani, 2019; Casas-Monroy et al., 2019). There is a variety of software for modelling distribution networks, with EPANET, Loop, and WaterCAD being the most prominent. But WaterGEMS has the most capabilities of all, and it was employed in this research (Kadhim, Abdulrazzaq & Mohammed, 2021).

Abdulsamad and Abdulrazzaq (2022) created a hydraulic network model using

✉hassan.almousawey2010m@coeng.uobaghdad.edu.iq

ArcMap 10.8 and WaterGEMS. The network's source nodes are measured with a handheld electronic ultrasonic flowmeter. Using a pressure gauge at eight junctions, the system was calibrated. The network's pressure varied from 8 to 21 m, while the main pipes' velocity was 0.5–2 $m \cdot s^{-1}$.

Patel, Sahoo and Mohanty (2020) used WaterCAD software to analyse the water distribution network in the municipality of Dilla town. Through simulation, fixed pressure reduction valves, also known as PRVs, were placed in the areas where they would be most efficient in lowering both the pressure and the amount of water lost to leakage. Initially, the existing system had an average water distribution pressure of 58 m when it was first built. The network was optimised, and as a result, the average pressure decreased to 44 m; therefore, the amount of leakage decreased by an average of 24%. According to the findings of the study, the implementation of PRVs in the water distribution system is a potentially useful method for minimising water loss due to leakage since it lowers the pressure in the water distribution networks.

Rai and Lingayat (2019) used EPANET software, the Hardy Cross methodology, and the Newton–Raphson method to analyse and distribute a water distribution system appropriately. Hydraulic variables such as pressure and flow were simulated. All flows and velocities were validated to be able to supply the network with an acceptable amount of water. By computing the residual head at each node using elevation as an input, researchers were able to deduce other significant flow parameters, including nodal demand, velocity, and residual head. The researchers discovered that complex networks could be addressed fast. Head loss decreases as the number of iterations increases, and the acquired values are checked by balancing flows at each point.

Hussien Al-Mansori, Mizhir Al-Fatlawi and Al-Zubaidi (2020) conducted a research in Iraq on Babylon University's pipe network to determine residual chlorine levels in drinkable water. This effort includes determining the number, position, and dose of needed onsite chlorine injection points in an effort to increase chlorine concentrations in the networks to acceptable levels. Between December 2016 and April 2017, 10 sample locations were chosen from Babylon University's water network. The concentration of residual chlorine was measured by taking samples three times a day, twice a week. The findings were evaluated in light of WHO criteria (World Health Organization [WHO], 2022). It was determined that the bulk decay coefficient is –1.18 daily while the wall decay coefficients range from –0.01 to –0.91 daily. The main conclusion of the study is that re-chlorination stations can be used to increase chlorine levels in the pipe network.

There is no previous research on the hydraulic performance and water quality of the water distribution network in Najaf city. The primary objective of this research is to evaluate the hydraulic capacities of Al-Nasir water distribution network in Al-Najaf Governorate through field measurements and the use of the WaterGEMS software. In addition, it intends to investigate and assess the chlorine deterioration in the distribution network.

Al-Mousawey, H., Abed, B. Sh. (2022). Simulation and assessment of water supply network for Al-Nasir network at Al-Najaf Governorate. *Sci. Rev. Eng. Env. Sci.*, *31* (3), 176–189. DOI 10.22630/srees.3373

Materials and methods

Study area

Abu-Talib, Al-Nasir, Al-Mohandisin, Old Milad, and Al-Fao Districts are located in the northern section of Al-Najaf Governorate, as shown in Figure 1. All of these districts are supplied by a single network. They have a combined surface area of 5.57 km^2, a population of 91,000 capita. According to the 2021 local estimation of population, drinking water in Al-Najaf city is treated by the main water treatment project of Al-Najaf city. Then water is pumped to the main pump station located approximately at the centre of the city, from there, seven mains distribute the water to the city, the network of the study area is supplied by a single main pipe of a 500 mm diameter, and two pumps pumping water to the specified network working alternatively for eight-hour period. All the pipelines in the network are tested for 10 bar working pressure.

For the current analysis, a water distribution network model was constructed that included main and secondary pipes, neglecting network laterals. The total pipe length of the network is 68.2 km.

Field measurements and observation data

The data and designs for the network infrastructure were received from the municipal authorities of the water supply, while additional data on the pump servicing the network and operating hours were gathered from

FIGURE 1. Area of study within Al-Najaf Governorate

FIGURE 2. The locations of fieldwork measurements

Najaf city's main pump station. To correctly generate the model utilising WaterGEMS––ArcGIS interface, GIS plans were obtained from the water department. At the end-user taps in 10 locations distributed along the network (shown in Fig. 2), pressure readings were performed using a glycerine-filled pressure gauge preceded by an air venting valve (shown in Fig. 3) connected directly to the first connection inside the house.

The measurements were performed during peak demand hours. For the assessment of residual chlorine, water samples were taken from the network using clean sampling bottles.

FIGURE 3. The apparatus used for the pressure head measurements

Determination of residual chlorine coefficients

The decrease of residual chlorine in the water distribution system occurs in both the bulk water and the pipe walls. The wall decay is a surface area process, whereas the bulk decay is a volume-based degradation process.

Bulk decay coefficient (K_b). Pipe characteristics have little impact on the bulk flow response coefficient. The chemical makeup

Al-Mousawey, H., Abed, B. Sh. (2022). Simulation and assessment of water supply network for Al-Nasir network at Al-Najaf Governorate. *Sci. Rev. Eng. Env. Sci.*, *31* (3), 176–189. DOI 10.22630/srees.3373

of water determines its qualities. To establish its value, a laboratory test was carried out (Ozdemir & Ucak, 2002; Mostafa, Matta & Halim, 2013). The laboratory tests were performed by collecting eight water samples from various locations, then, each water sample was split into 13 parts, and the Lovibond Comparator 2000+ device was used to measure residual chlorine concentration.

At time zero, the first sample was measured. Then, the remaining samples were tested at one-hour intervals, and the findings were plotted against time, as seen in Figure 4. This method was performed on all eight water samples to achieve the most consistent results.

The first-order decay model assumes that the chlorine concentration will decline exponentially and is the most widely used one (Hua, West, Barker & Forster, 1999; Castro & Neves, 2003).

According to the equation $C = C_0 e^{-kt}$, where C is the chlorine concentration at the time (t), C_0 is an initial chlorine concentration, k is the decay rate in min^{-1}, t is the time in min. The calculated bulk decay coefficient was taken to be equal to -0.095 h^{-1}, which has the highest regression rate ($R^2 = 0.9867$) and corresponds to -2.28 day^{-1}. The negative sign refers to the reduction of residual chlorine with time.

Wall decay coefficient (K_w). The coefficient of wall deterioration is governed by the condition of the pipe wall and the lining material. It is affected by the interaction between the bulk flow and the wall contact. The mass transfer coefficient, which is based on the molecular diffusivity of the measured material, influences the bulk pipe flow rate. Amount of $1.44 \cdot 10^{-9}$ $m^2 \cdot s^{-1}$ is the chlorine diffusivity at a water temperature of 25°C. The network comprises PVC-HDPE and ductile iron pipes; however, because the network is less than 10 years old, the K_w value for the PVC pipes is assumed to be zero. The expected K_w value for ductile iron pipes is equal to -4 $mg \cdot m^{-2} \cdot day^{-1}$ (Nagatani et al., 2008). Then the value of K_w was adjusted until an acceptable level of fitness was achieved.

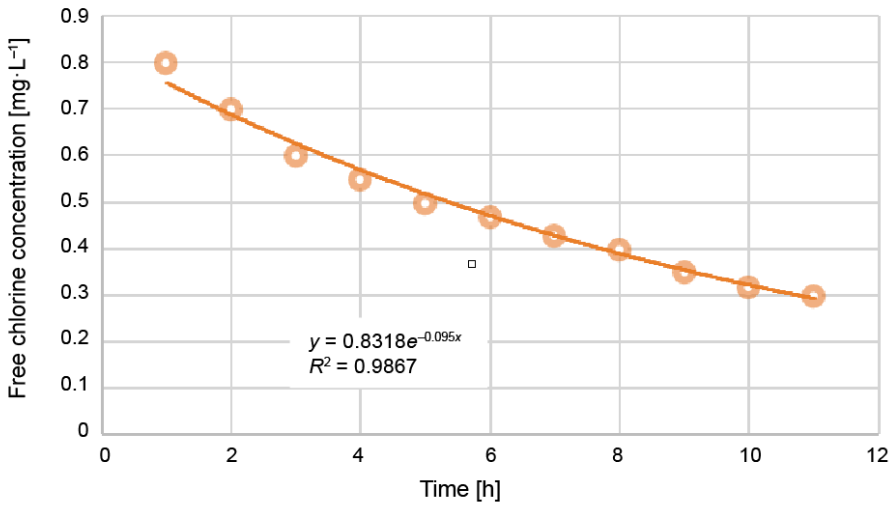

FIGURE 4. First-order adjustment of the testing results

Bentley WaterGEMS

Windows application WaterCAD was designed by Haestad Methods Inc. of Cincinnati, Ohio. WaterGEMS is the most recent version of the WaterCAD software, and it is a straightforward program for simulating or designing water distribution networks. WaterGEMS offers a thorough yet user-friendly decision-support tool for water distribution networks. The software helps you gain a better understanding of how infrastructure functions as a system, how it responds to operational scenarios, and how it should expand as population and demand rise. Engineers and utilities may use WaterGEMS to evaluate, build, and improve water distribution systems in the areas of discharge, pressure head, constituent concentration analysis, and pump simulation in different scenarios, with the condition that accurate network data is available to create an accurate model that truly represents the network under study (Haestad Methods Inc., 2003). Figure 5 illustrates the flowchart and required input data for WaterGEMS software.

In the current investigation, the Hazen–Williams head loss formula is utilised to calculate the amount of hydraulic head loss produced by friction with pipe walls. The reservoir's features, pipelines, connections, valves, and pumps were correctly modelled, and the system's demand was determined based on 350 L per capita daily. The demand of each distribution network junction was then determined based on the region covered by the individual junction. Pipe features were entered along with pump characteristics and valve properties. The network pipes are comprised of cement-lined ductile iron pipes with 500 and 300 mm diameters and PVC-HDPE pipes with 225 and 160 mm diameters. Since

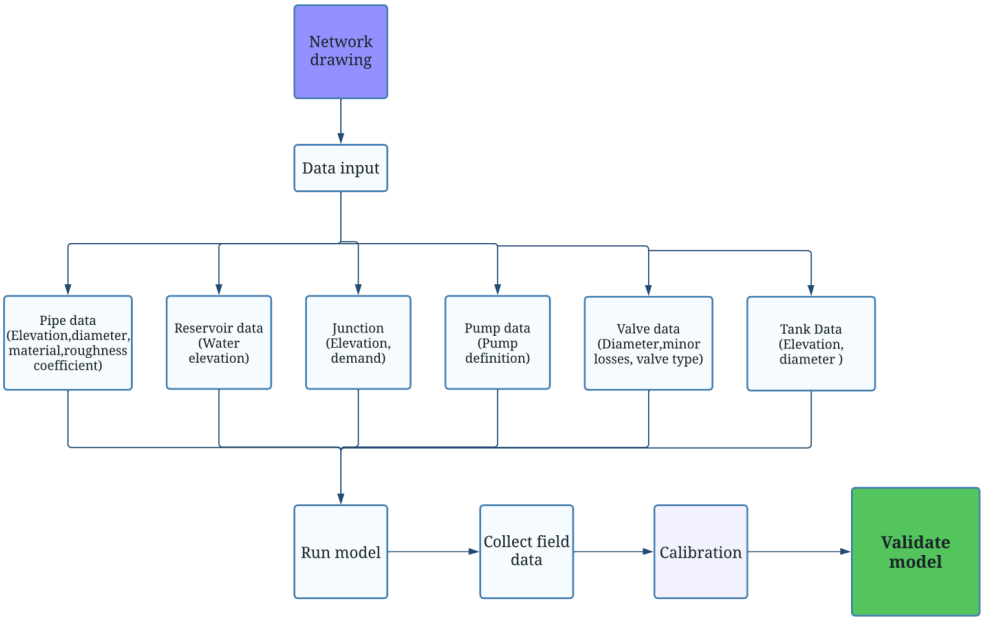

FIGURE 5. WaterGEMS software flowchart

Al-Mousawey, H., Abed, B. Sh. (2022). Simulation and assessment of water supply network for Al-Nasir network at Al-Najaf Governorate. *Sci. Rev. Eng. Env. Sci.*, *31* (3), 176–189. DOI 10.22630/srees.3373

the network is fairly new (less than 10 years old), the typical roughness coefficient (*C*) for the two types of pipes was assumed to be 120 and 150, respectively (Chin, Mazumdar & Roy, 2000; Jalal, 2008).

Model calibration

The calibration of a hydraulic model is to ensure the model's dependability. This phase in the modelling process entails fine-tuning a model until it matches field data over a specified period so that it may be used to predict system performance and evaluate alternative approaches (Sun & Sun, 2015; Hessling, 2017; Farhan & Abed, 2021). This process involves slight adjustments to the input values to generate output values that accurately represent the system (Khudair, 2015; Parady, Ory & Walker, 2021). Throughout the water distribution network, pressure head measurements are monitored and utilised to calibrate the pressure head levels. Multiple variables might affect pressure values. As a consequence, calibration may be accomplished by just adjusting the internal pipe roughness values or nodal demand predictions until adequate fitness is obtained between the observed and simulated pressure heads and flow values. This idea is based on the fact that pipes (*C*) values and system demands are often estimated, allowing space for error, in contrast to pipe lengths and diameters, which are measured directly. The calibration procedure was performed between 4 and 5 AM during peak demand hours by slightly adjusting total system demand. Three sets of measurements were performed on three different days during peak demand hours. Results of measurements varied slightly. Thus, the data set having the highest *RMSE* value was selected to represent the calibration procedure.

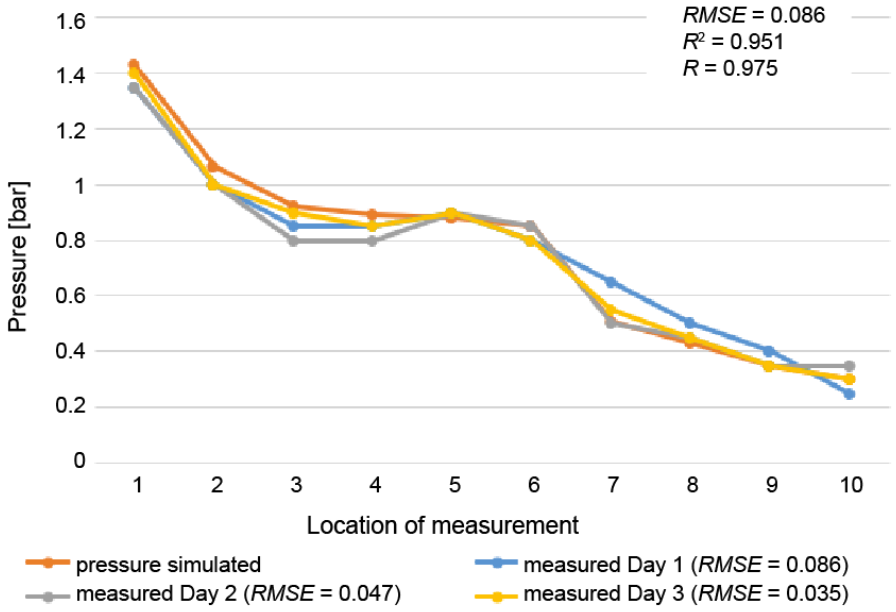

FIGURE 6. Comparison between simulated and measured pressure heads along different junctions

When comparing the observed and simulated pressure head values, the root mean squared error (*RMSE*), *R*-squared correlation (R^2) and the Pearson correlation coefficient (*R*) were used to demonstrate how close the two data sets were. Figure 6 compares measured and simulated pressure values with low *RMSE* values of 0.086 and high *R* and R^2 values of 0.975 and 0.951, respectively, indicating good agreement between simulated and observed values. On the other hand, the model was calibrated to provide an approximation of the wall decay coefficient (K_w), which was assumed to be –4 mg·m^{-2}·day^{-1} (as was mentioned earlier), value –2.3 mg·m^{-2}·day^{-1} was determined by trial and error to be the value for K_w that yielded the most plausible results in simulating the actual measurements in the network. For simulating residual chlorine concentrations, the model was calibrated similarly based on the results of concentration tests on 10 samples collected from various places within the network for three days. Figure 7 illustrates the comparison between computed and field measured chlorine samples at maximum consumption hours with low *RMSE* value of 0.057 and high *R* and R^2 values of 0.917 and 0.84, respectively which shows high agreement between observed and simulated values.

Model verification

Similarly to the calibration process, three sets of field measurements on three different days were carried out to gather pressure head readings at various points throughout the network during the hours of moderate water usage between 10 and 11 AM. Flow-rate measurements were made at the location of the pump station and some other locations using an ultrasound flowmeter to estimate system demand. This was done to ensure the accuracy of the simulation of the modelled distribution network. Additionally, residual chlorine concentrations were measured at

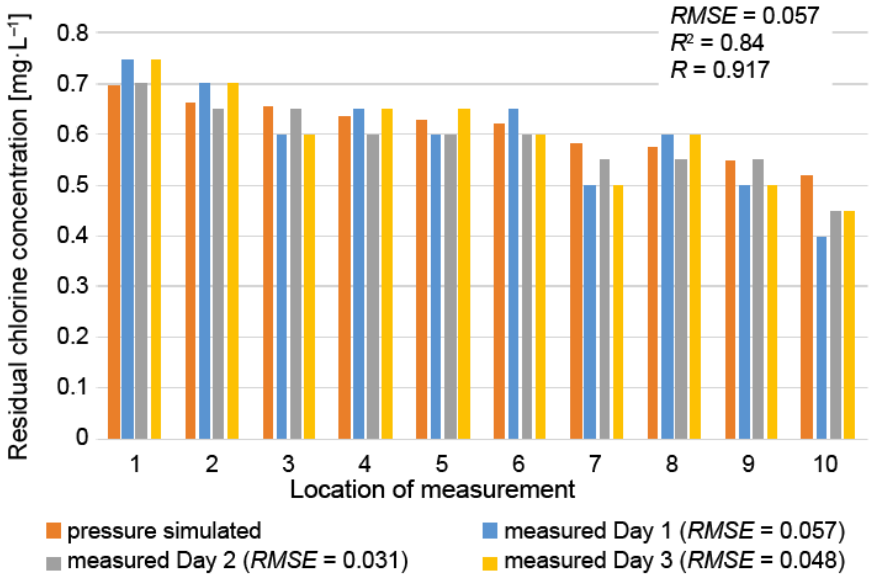

FIGURE 7. Comparison between simulated and field-measured residual chlorine concentrations

Al-Mousawey, H., Abed, B. Sh. (2022). Simulation and assessment of water supply network for Al-Nasir network at Al-Najaf Governorate. *Sci. Rev. Eng. Env. Sci.*, *31* (3), 176–189. DOI 10.22630/srees.3373

field measurement sites. The measurement set with the highest *RMSE* value was selected to represent the verification process. Table 1 compares the field observed to simulated pressure values, and the verification process' findings suggest that there is strong agreement between these measurements because of the negligible difference and low value of *RMSE* of 0.095 and high *R* and R^2 values of 0.985 and 0.97, respectively.

Table 2 compares the observed and simulated residual chlorine concentrations. The results indicate that the difference between the observed and simulated residual chlorine concentrations is low, and that the simulation achieves close results to the observed concentrations due to the small *RMSE* value of 0.05 and good *R* and R^2 values of 0.819 and 0.671, respectively.

TABLE 1. Comparison between calculated and measured pressure heads at various nodes

Node ID	Simulated pressure [bar]	Measured pressure [bar]	*RMSE*	R^2	*R*
J-1884	1.45	1.5	0.095	0.97	0.985
J-1900	1.446	1.5			
J-1910	1.3	1.4			
J-1888	1.284	1.25			
J-1886	1.281	1.2			
J-1908	1.254	1.25			
J-1906	1.112	1			
J-1904	1.066	1			
J-1894	0.987	0.85			
J-1896	0.902	0.75			

TABLE 2. Comparison between simulated and observed residual chlorine concentrations

Node ID	Simulated residual chlorine [mg·L^{-1}]	Measured residual chlorine [mg·L^{-1}]	*RMSE*	R^2	*R*
J-1894	0.686	0.7	0.05	0.671	0.819
J-1886	0.644	0.65			
J-1896	0.632	0.65			
J-1888	0.624	0.5			
J-1884	0.589	0.6			
J-1906	0.578	0.55			
J-1908	0.536	0.55			
J-1904	0.519	0.55			
J-1910	0.494	0.5			
J-1900	0.484	0.4			

Consequently, the hydraulic and residual chlorine simulation data may be relied upon when analysing the water distribution system.

Results and discussion

Pressure heads analysis

Using WaterGEMS software, a pressure heads analysis of the distribution network was carried out under steady-state circumstances during peak water demand hours, moderate water demand hours, and low water consumption hours. It was discovered that during the peak water demand hours, one pump was operating over its intended operating capability, mostly because of increased water use and continuous running of domestic pumps inside homes. Most network pressure heads were below acceptable levels, particularly at the centre of the network, and their values ranged from 0.2 to 1.3 bar; however, some junctions in the network had acceptable values of water pressure of 1.3––2 bar. This decrease in the pumping head is caused by the pump reaching its maximum discharge point due to increased demand. The simulation results show that the pressure heads for hours of moderate water demand are between 0.9 and 1.6 bar. For the third flow condition, which represents low water demand, the pressure heads reached the designed level because there was less water use and the domestic household tanks were full at this time. The pressure values were between 1.42 and 2.7. From field observation, most homes have their own pumps, which causes the water pressure in the network to drop, especially as the distance from the pumping station goes up. In Figures 8 and 9, a contour

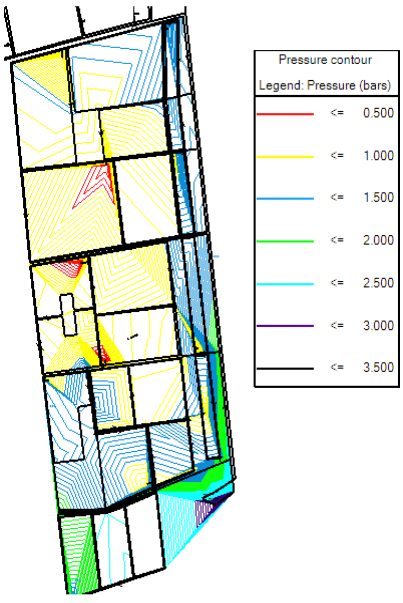

FIGURE 8. Contour map of pressure heads during maximum water demand

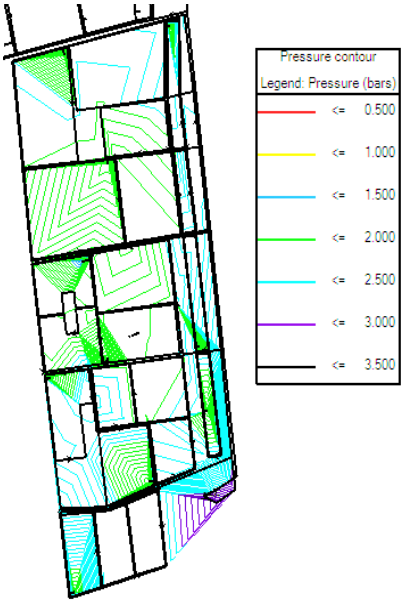

FIGURE 9. Contour map of the pressure heads during low water demand

Al-Mousawey, H., Abed, B. Sh. (2022). Simulation and assessment of water supply network for Al-Nasir network at Al-Najaf Governorate. *Sci. Rev. Eng. Env. Sci.*, *31* (3), 176–189. DOI 10.22630/srees.3373

profile shows the different pressure ranges in the network for different flow conditions. A possible solution for the present network's low pressures is to replace the existing pump with a newer model (locally obtainable) with a capacity of 3,000 $m^3 \cdot h^{-1}$ instead of the current one (1,200 $m^3 \cdot h^{-1}$). This upgraded pump will be able to supply the appropriate pressure at the network's near-end connectors. Figure 10 depicts the simulation result of the suggested method, with the lowest pressure value of 1.6 bar at maximum demand.

Velocity analysis

The simulation analysis shows that during maximum water demand, the flow velocities ranged between 0.5 and 2.59 $m \cdot s^{-1}$ for ductile iron pipes of 500 and 300 mm. The velocities in the PVC-HDPE pipes of 225 mm ranged between 0.1 and 2.65 $m \cdot s^{-1}$; the drop of velocity in some of the 225 mm pipes is due to unrequired extra piping in some locations. The velocity values for 160 mm PVC-HDPE pipes ranged between

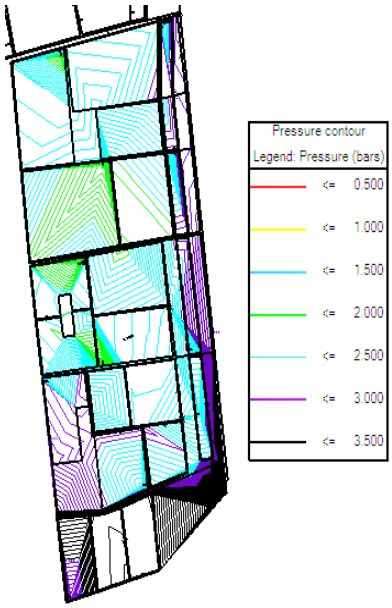

FIGURE 10. Pressure heads with improved pump at maximum demand

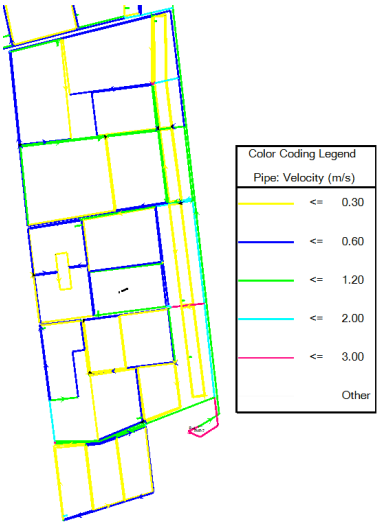

FIGURE 11. The ranges of velocities in the water distribution system at maximum water demand

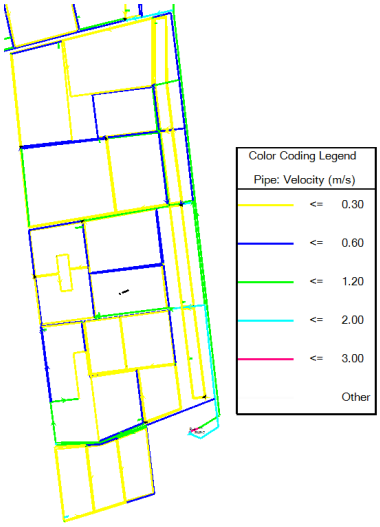

FIGURE 12. The ranges of velocities in the water distribution system at minimum water demand

0.1 and 1 $m \cdot s^{-1}$. These values of flow velocity revealed that the velocity in the ductile pipes is mainly within the allowable limits for all times, while the velocity in the lateral pipes exceeds the allowable limit in the low demand periods and decreases to be below the permissible limit in the dead flow junctions. Figures 11 and 12 show the velocity distribution for the distribution system for high and low water demand periods.

Residual chlorine analysis

During maximum demand period, the values of residual chlorine in the network were in the range of 0.5–0.8 $mg \cdot L^{-1}$, decreasing as the water reaches the middle parts of the distribution network. These ranges of residual chlorine are considered acceptable by local and international standards in terms of low limits but exceed the upper limit of 0.5 $mg \cdot L^{-1}$. The contour profile in Figure 13 shows the concentrations of residual chlorine throughout the network. During low demand period, the values of residual chlorine concentrations ranged between 0.45 and 0.76 $mg \cdot L^{-1}$, which exceeded the upper limit according to international standards (0.2––0.5 ppm) (WHO, 2022). Figure 14 shows the contour profile of residual chlorine concentrations during low demand period.

Conclusions

The network simulation using WaterGEMS software proved successful, with *RMSE* values ranging between 0.08 and 0.1, and 0.05 and 0.06 for the two simulations, respectively. It was revealed that there is a deficit in water pressure values nearly at the centre of the WDS, where the pressure heads drop below 1 bar due to the current one pump operation, particularly during peak demand hours; however, when there was less demand, the network performed adequately, and water pressure values were between 1.42 and 2.7 bar. Velocity in the main pipes of the distribution network is acceptable. However, velocity might increase or decrease in lateral

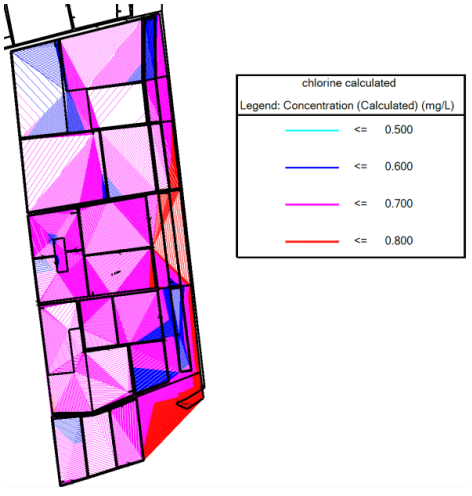

FIGURE 13. Values of residual chlorine during maximum demand period

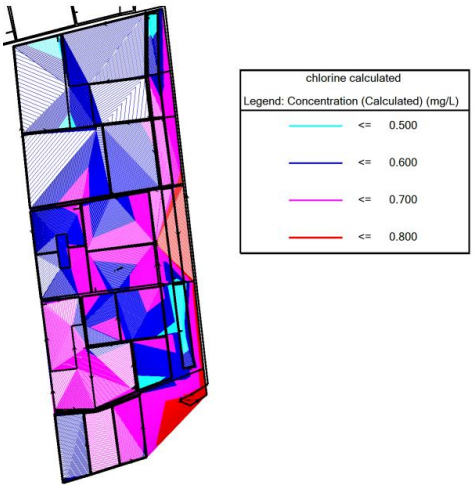

FIGURE 14. Values of residual chlorine during low demand period

pipes because of factors such as low demand or dead junctions. The pump that supplies the distribution network has inadequate specifications and cannot run within its optimal range. The simulation also showed that the residual chlorine levels were above the lower permissible limits at most locations throughout both testing periods, between 0.45 and 0.8 ppm.

References

Abdulsamad, A. A. & Abdulrazzaq, K. A. (2022). Calibration and analysis of the potable water network in the Al-Yarmouk region employing WaterGEMS and GIS. *Journal of the Mechanical Behavior of Materials*, *31* (1), 298–305.

Albadry, A. M. a. (2017). The effect of the utilitarian need for the high water tanks towers to sustain life in the City. *Journal of Engineering*, *23* (2), 20–38. Retrieved from: https://www.joe.uobaghdad.edu.iq/index.php/main/article/view/75 [accessed 23.07.2022].

Alsaydalani, M. O. A. (2019). Simulation of pressure head and chlorine decay in a water distribution network: a case study. *The Open Civil Engineering Journal*, *13* (1), 58–68.

Bashar, K. edin E., Khudair, B. H., & khalid, G. khalaf (2015). Calibration and Verification of the Hydraulic Model for Blue Nile River from Roseires Dam to Khartoum City. *Journal of Engineering*, *21* (12), 46–62. Retrieved from https://joe.uobaghdad.edu.iq/index.php/main/article/view/289 [accessed 23.07.2022].

Casas-Monroy, O., Byllaardt, J. van den, Bradie, J., Sneekes, A., Kaag, K. & Bailey, S. A. (2019). Effect of temperature on chlorine treatment for elimination of freshwater phytoplankton in ballast water: bench-scale test. *Canadian Journal of Fisheries and Aquatic Sciences*, *76* (10), 1768–1780.

Castro, P. & Neves, M. (2003). Chlorine decay in water distribution systems case study – lousada network. *Electronic Journal of Environmental, Agricultural and Food Chemistry*, *2* (2), 261–266.

Chin, D. A., Mazumdar, A. & Roy, P. K. (2000). *Water-resources engineering* (Vol. 12). Hoboken: Prentice Hall Englewood Cliffs.

Farhan, A. A. & Abed, B. S. (2021). Estimation of surface runoff to Bahr Al-Najaf. *Journal of Engineering*, *27* (9), 51–63. https://doi.org/10.31026/j.eng.2021.09.05

Haestad Methods Inc. (2003). *Haestad Methods WaterCAD Version 6 User's Manual*. Waterbury: Haestad Methods Inc.

Hessling, J. P. (2017). *Uncertainty quantification and model calibration*. London: Intech Open.

Ho, H. C., Puika, K. S. & Kasih, T. P. (2020). Development of IoT-based water reduction system for improving clean water conservation. *Scientific Review Engineering and Environmental Studies (SREES)*, *29* (1), 54–61. https://doi.org/10.22630/PNIKS.2020.29.1.5

Hua, F., West, J. R., Barker, R. A. & Forster, C. F. (1999). Modelling of chlorine decay in municipal water supplies. *Water Research*, *33* (12), 2735–2746.

Hussein, H. A. (2021). *Evaluation and analysis the effects of some parameters on the operation efficiency of the main water pipe in Karbala City using WaterCAD program*. Baghdad: Ministry of Higher Education.

Hussien Al-Mansori, N. J., Mizhir Al-Fatlawi, T. J. & Al-Zubaidi, L. S. A. (2020). Equilibrium of Babylon water supply network using EPANET program. *Plant Archives*, *20* (2), 693–700.

Jalal, M. M. (2008). *Performance Measurement of Water Distribution Systems (WDS). A critical and constructive appraisal of the state-of-the-art* (master thesis). University of Toronto, Toronto.

Kadhim, N. R., Abdulrazzaq, K. A. & Mohammed, A. H. (2021). Hydraulic analysis and modelling of water distribution network using WATERCAD and GIS: Al-Karada Area. *E3S Web of Conferences*, *318*, 04004.

Mostafa, N. G., Matta, M. E. & Halim, H. A. (2013). Simulation of chlorine decay in water distribution networks using EPANET – case study. *Simulation*, *3* (13), 100–116.

Nagatani, T., Yasuhara, K., Murata, K., Takeda, M., Nakamura, T., Fuchigami, T. & Terashima, K. (2008). *Residual chlorine decay simulation in water distribution*

system. The 7th International Symposium on Water Supply Technology. Yokohama, Japan, 22–24.

Ozdemir, O. N. & Ucak, A. (2002). Simulation of chlorine decay in drinking-water distribution systems. *Journal of Environmental Engineering*, *128* (1), 31–39.

Parady, G., Ory, D. & Walker, J. (2021). The overreliance on statistical goodness-of-fit and under-reliance on model validation in discrete choice models: A review of validation practices in the transportation academic literature. *Journal of Choice Modelling*, *38*, 100257.

Patel, O. S., Sahoo, B. & Mohanty, S. (2020). Water distribution system modeling to reduce leakage. *Juni Khyat*, *10* (12), 207–214.

Rai, R. K. & Lingayat, P. (2019). Analysis of water distribution network using EPANET. *Proceedings of Sustainable Infrastructure Development & Management (SIDM)*. http://dx.doi.org/10.2139/ssrn.3375289

Summeren, J. van & Blokker, M. (2017). Modeling particle transport and discoloration risk in drinking water distribution networks. *Drinking Water Engineering and Science*, *10* (2), 99–107.

Sun, N. Z. & Sun, A. (2015). *Model calibration and parameter estimation: for environ mental and water resource systems*. Berlin: Springer.

World Health Organization [WHO] (2022). *Guidelines for drinking-water quality* (4th ed.). Geneva: World Health Organization.

Summary

Simulation and assessment of water supply network for Al-Nasir network at Al-Najaf Governorate. This study simulates and assesses the hydraulic features and residual chlorine in Al-Najaf city's water supply network using WaterGEMS. Field and laboratory work was done to determine pressure heads, velocities, and chlorine residual. Constructed model was validated using field data. Values of *RMSE* were between 0.08 and 0.1, and 0.05 and 0.06 for pressure and residual chlorine, respectively. The examination of water distribution system (WDS) during peak demand hours indicated that the pump unit's capacity could not meet the high-water demand, resulting pressure loss with values between 0.1 and 2 bar. Simulated residual chlorine levels ranged between 0.45 and 0.8 ppm.

Scientific Review Engineering and Environmental Sciences (2022), 31 (3), 190–202

Sci. Rev. Eng. Env. Sci. (2022), 31 (3) https://srees.sggw.edu.pl

ISSN 1732-9353 (suspended) eISSN 2543-7496 DOI 10.22630/srees.3375

Received: 04.08.2022
Accepted: 20.09.2022

Safa MUSTAFA[1]

Mohammed Aziz HAMEED[1]

Anmar DULAIMI[1, 2, 3]✉

[1]Ministry of Education, Karbala, Iraq
[2]University of Warith Al-Anbiyaa, College of Engineering, Karbala, Iraq
[3]Liverpool John Moores University, School of Civil Engineering and Built Environment, Liverpool, UK

EVALUATION OF THE PROPERTIES OF MODIFIED LOCAL ASPHALT BINDER BY USING STYRENE BUTADIENE RUBBER (SBR) OR LOW-DENSITY POLYETHYLENE (LDPE)

Key words: asphalt binder, polymers, SBR, LDPE, rheological properties

Introduction

Bitumen is one of the earliest engineering materials known to humanity (Whiteoak, Read & Hunter, 2003). Asphalt is a cementitious material that ranges from dark brown to black and is mostly composed of high molecular weight hydrocarbons, although asphalt is portrayed as a low-value byproduct, these heavy fractions of petroleum were among the first oil-derived compounds having applications in human history in various ways such as construction industry, medicine and jewellery adhesives. If one considers that asphalt is the most commonly used material for paving roadways, in addition to a joint sealant for waterproofing material and roofing applications, the significance of asphalt becomes evident (Hardin, 1995; Singh, Tarannum & Gupta, 2003; Speight, 2016). The present global bitumen consumption is over 102 million tonnes per year, with 85% of that used in various types of pavements (Mostafa, Tawhed & Elshahat, 2016). The quality of generated asphalt is intrinsically tied to refinery operations and crude oil sources. Some good bitumen qualities can be attained by selecting good petroleum or using correct refinery techniques. Due to limited petroleum for manufacturing high-

✉A.F.Dulaimi@ljmu.ac.uk; a.f.dulaimi@uowa.edu.iq

-quality bitumen and an absence of efficient control actions through the refinery process, in addition to the economic benefits, industries have focused increasing attention on bitumen modification (Zhu, Birgisson & Kringos, 2014). Furthermore, the pavement and waterproofing industries have grown quickly around the world in recent decades, particularly in developing countries (Presti, 2013). Asphalt's rheologic qualities such as viscoelastic, adhesion and durability are significant when considering it as a paving material (Cao et al., 2018; Abduljabbar et al., 2022). Polymers-modified asphalt gained popularity in the second half of the twentieth century and are now essential in limiting the deterioration of road networks and intervention in modern waterproofing industries (Polacco, Filippi, Merusi & Stastna, 2015; Hameed, Al-Busaltan, Dulaimi, Kadhim & Al-Yasari, 2021). Due to increased traffic in Iraq because of the growing growth of uncontrolled vehicles and extreme weather conditions due to global climate change, many defects such as high-temperature rutting (permanent deformities) and low temperature cracking or fatigue cracking. It is obvious that most roads in Iraq suffer higher deformation at high ambient temperatures and when traffic is slow or stationary (Abed, Hamdou & Ahmed, 2011; Abbas, 2017; Chopra, Parida, Kwatra & Chopra, 2018). The bitumen is responsible for the visco-elastic behaviour characteristic of asphalt when mixing the polymer with bitumen and plays a prime role by increasing the elastic component of the bitumen thereby reducing the viscous component. It also influences a variety of features of road performance, including resistance to permanent deformation and cracking (Whiteoak et al., 2003). During the last four decades, an increasing number of studies have focused on polymer modification of asphalt, and a rapidly growing number of research papers have been published that investigated various polymer modifications to improve the quality and performance of asphalt pavement, such as thermoplastic elastomers, e.g.: styrene isoprene styrene (SIS), styrene butadiene styrene (SBS), and plastomers, e.g.: ethylene-butyl acrylate (EBA) and polypropylene (PP) polyethylene (PE) (Al-Hadidy & Yi-Qiu, 2009; Mazumder, Siddique, Ahmed, Lee & Lee, 2020; Alghrafy, El-Badawy & Abd Alla, 2021; Babagoli, 2021; Che et al., 2022). According to various research, the mixing temperature for a homogeneous blend should range from 150° to 230°C, with a typical range of 175–200°C, for a period of 30 min to 4 h. The temperature at which the blend becomes a homogeneous polymer with asphalt solution is directly related to the asphalt binder's polymer concentration and asphaltenes content (Ahmed & Al-Harbi, 2014; Babagoli, 2021). The modification of bitumen using thermoplastic elastomers, of the four major groups of thermoplastic elastomers–polyether-polyester copolymers, polyurethane, styrenic block copolymers, and olefinic copolymers is the styrenic block copolymers that have proved to present the greatest potential when blended with bitumen (McNally, 2011). Styrene butadiene rubber (SBR) is a representative of elastomers (Whiteoak et al., 2003). Increased elasticity, higher adhesion and cohesion qualities of the binders, and a lower rate of oxidation are all benefits of using SBR in mixes (Roque, Birgisson, Tia, Kim & Cui, 2004), this revealed why SBR has been widely used as an important asphalt

modifier. Many studies show the addition of polymer (SBR) considered one of the asphalt improvement solutions techniques has been used in several countries (Sadhu & Bhowmick, 2004; Chakraborty et al., 2010; Zhang & Yu, 2010; Ameri, Vamegh, Rooholamini & Haddadi, 2018). These researchers discovered that SBR modified asphalt mixtures could produce exceptional pavement performance, including anti-rutting, anti-cracking, and moisture resistance, which was even better than SBS modified asphalt mixtures (Ren et al., 2018). Polyethylene (PE) is a representative of plastomer and it is the most often used non-rubber thermoplastic polymer in modified road binders. Thermoplastics are defined by their ability to soften when heated and rigid when cooled (Whiteoak et al., 2003; Polacco, Stastna, Biondi & Zanzotto, 2006). The penetration of these polymers is more important than the softening point, which is the reverse of thermoplastic elastomers. Several researches have already been completed on the compound modification of asphalt binder utilizing PE in road and roofing applications (Fang, Li, Zhang & Wang, 2008; Navarro, Partal, Martinez-Boza & Gallegos, 2010; Liang et al., 2021).

It was found that using 1.5 wt% of polypropylene fibres could importantly increase the impact resistance of lightweight concrete and improve the compressive and flexural strengths at the same time (Orouji, Zahrai & Najaf, 2021; Najaf, Abbasi & Zahrai, 2022). Recycled polypropylene fibre had a compressive and tensile strength of roughly 1.7 and 1.6 times in comparison to the reference samples (Najaf, Orouji & Zahrai, 2022).

Rheological criterion and morphology revealed that low-density polyethylene (LDPE) has the best compatibility with asphalt, whereas high-density polyethylene (HDPE) has the worst compatibility. More branched PE has lower density and crystalline, resulting in a more homogeneous dispersion in microscopy and better compatibility (Liang et al., 2021). Finally, bitumen is a low-cost thermoplastic material that is utilized in roofing, road, and pavement applications. A study was done on the characteristics of LDPE asphalt mixtures. As a result of the addition of LLDPE, rotational viscosity, softening point, elasticity, and penetration index increased, but permanent deformation and penetration were reduced (Nizamuddin, Jamal, Gravina & Giustozzi, 2020).

Currently, there is a rapid usage of different materials to enhance the performance of the asphalt binder. The major objective of this research is to examine the possibility of using low-density polyethylene (LDPE) and styrene butadiene rubber (SBR) as additives for conventional asphalt binder (unmodified asphalt binder). Given that increasing attention has been given to using SBR or LDPE to manufacture asphalt pavements, this paper will examine the feasibility of the use of SBR or LDPE as an additive to the asphalt binder. In addition, the performance of the asphalt binder containing SBR or LDPE has not been fully considered to date. Different percentages of SBR and LDPE (3, 5, 7 and 9%) were added to conventional asphalt for the preparation of modified asphalt. The properties of virgin and modified asphalt binder were considered, counting penetration, viscosity and ductility and effects of available additive polymer with the suitable amount, on the properties of asphalt binder and compared these properties with virgin unmodified asphalt binder.

Materials and test methods

Asphalt binder

The used asphalt binder is 40–50 penetration grade that is obtained from Al-Daurah refinery. The asphalt binder's physical parameters and tests are listed in Table 1. These experiments were carried out in the laboratory of the Al-Daurah refinery, which is located southwest of Baghdad.

TABLE 1. Physical properties of asphalt binder used in this study (Ministry of Oil, Midland refineries company, Al-Daurah refinery, 2021)

Performance index	Unit	Value
Penetration at 25°C (100 g, 5 s) (0.1 mm)	1/10 mm	49
Ductility at 25°C (5 cm·min^{-1})	cm	97
Softening point	°C	50
Specific gravity at 25°C	–	1.02
Flash point (Cleveland open cup)	°C	285

Styrene butadiene rubber (SBR) and low-density polyethylene (LDPE)

In this study, two types of polymers are used styrene butadiene rubber (SBR) and low-density polyethylene (LDPE). At all temperatures, SBR is a random copolymer of styrene and butadiene that has a considerable impact on the outcomes of ductility and elastic recovery tests (Johnston & King, 2008). It is obtained locally from tires factory in Al-Najaf governorate and has a name SBR1502. The LDPE is a plastomers polymer, a white granule that is utilized in the tires industry and other private manufacturers in Iraq to make plastic belts.

Two asphalt binders (40–50; modified and unmodified binders) used in this study were prepared by a supplier from the same asphalt. The modified asphalt binder is prepared by adding four percentages of the polymer SBR (3, 5, 7 and 9%) and four percentages of the polymer LDPE (3, 5, 7 and 9%) by weight of the asphalt binder. The physical properties of polymer SBR and LDPE are in Tables 2 and 3. Figure 1 shows photos of the SBR and LDPE polymer samples.

TABLE 2. Physical properties and specification of styrene butadiene rubber SBR1502 (Company for Tire Industry, 2021)

Performance index	Unit	Value
Specific gravity	–	0.95
Tensile strength (σ_t)	MPa	23 min
Modulus at 300% ext.	MPa	1–23
Bound styrene	%	23.5 +1.0 max
Melting point	°C	200 ±10
Elongation at break	%	340 min
Viscosity ML (1 + 4) 100°C	M.U.	52 ±3
Organic acid	%	4.7–7.2

TABLE 3. Physical properties and specification of low-density polyethylene (State Company for Petrochemical Industry in Basrah City, 2008)

Performance index	Unit	Value
Specific gravity	–	0.922
Tensile strength at break	MPa	21
Tensile strength at yield	MPa	9
Melt index	g per 10 min	0.33
Elongation at break	%	310
Melting point	°C	170
1% secant modulus	MPa	175

Mustafa, S., Hameed, M. A., Dulaimi, A. (2022). Evaluation of the properties of modified local asphalt binder by using styrene butadiene rubber (SBR) or low-density polyethylene (LDPE). *Sci. Rev. Eng. Env. Sci.*, *31* (3), 190–202. DOI 10.22630/srees.3375

a b

FIGURE 1. Styrene butadiene rubber SBR1502 (a) and low-density polyethylene (b)

Preparation of specimens

The modified asphalts were prepared by using a blending machine, SBR1502 and LDPE were blended with asphalt binder by using a wet process (Al-Bana'a, 2010). The asphalt binder was first heated in a container until it became fluid, and then when it reached 170–190°C the SBR1502 and LDPE were added. The mixing time was 60 min and the mixing speed was 4,000 rpm in the laboratory (Kim, Mazumder, Lee & Lee, 2018; Mazumder et al., 2020; Liang et al., 2021).

Physical properties test

The physical properties of asphalt binder, including (softening point test, penetration test and ductility test), were tested following designations AASHTO T 51-09, T 53-09 and T 49-15 specifications respectively (American Association of State Highway and Transportation Officials [AASHTO], 2013a, 2013b, 2015).

Softening point test apparatus

This apparatus measures the softening point of asphalt binder materials whose softening ranges between 30° and 200°C). The temperature at which the asphalt sample descends a distance of 2.54 cm, when heated at a speed of 5°C·min^{-1}, is known as the softening point.

Penetration test apparatus

Penetration is a measure of the hardness of asphalt binder, as this device measures the penetration of solid and semi-solid asphalt materials, the penetration of a typical needle through an asphalt binder sample under the following conditions: load of 100 g, temperature of 25°C (77 F) and time of 5 s.

Ductility test apparatus

This device measures the distance that asphalt binder materials can be stretched when exposed to the impact of clouds at a constant

speed of 5 cm·min^{-1} until the asphalt sample is cut off, and the total distance of this device reaches 150 cm.

Results and discussion

The findings of the tests on the asphalt binder, comprising several quantities of styrene butadiene rubber (SBR) polymer and low-density polyethylene (LDPE) are reported in Table 4. Figures 2 and 3 show the impact of SBR and LDPE content on the softening point and penetration of the asphalt binder. Different contents of SBR and LDPE are selected to show the impacts on the softening point of asphalt under constant SBR or LDPE content. It can be seen that the softness point increases with increasing SBR or LDPE concentration. The softening point improved from 55° to 70°C when SBR increased from 3 to 9%. While the increase of LDPE from 3 to 9% results in an increase in the softening point from 53° to 60°C. This means that SBR has a better performance in comparison to the LDPE at the same content (9%). These results are consistent with Alghrafy et al. (2021) and Babagoli

TABLE 4. Physical properties of the original and modified asphalt binder with different percentages of styrene butadiene rubber (SBR) and low-density polyethylene (LDPE)

Test method	Neat	SBR content				LDPE content			
		3%	5%	7%	9%	3%	5%	7%	9%
Softening point [°C]	52	55	59	65	70	53	56	57	60
Penetration at 25°C [dmm]	49	44	41	34	36	40	34	31	26
Ductility [cm]	110	120	155	175	190	105	100	80	70
Penetration index (*PI*)	–1.0	–0.3	0.4	1.1	2	–1.0	–0.7	–0.6	–0.4

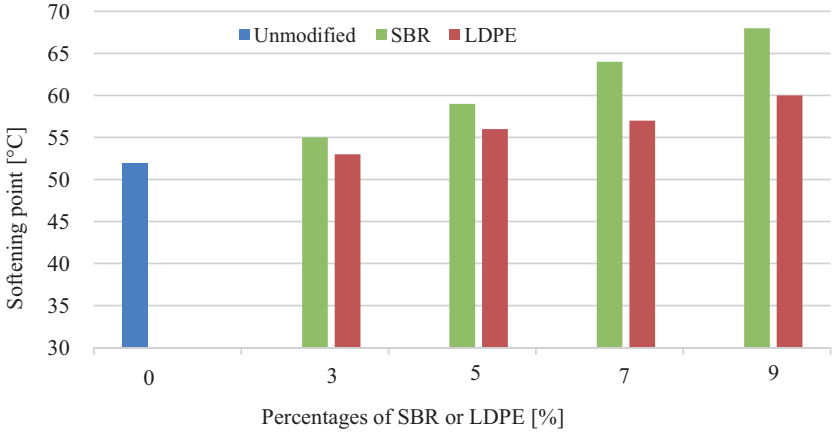

FIGURE 2. The softening point of asphalt with various styrene butadiene rubber (SBR) or low-density polyethylene (LDPE) contents

Mustafa, S., Hameed, M. A., Dulaimi, A. (2022). Evaluation of the properties of modified local asphalt binder by using styrene butadiene rubber (SBR) or low-density polyethylene (LDPE). *Sci. Rev. Eng. Env. Sci.*, *31* (3), 190–202. DOI 10.22630/srees.3375

(2021). The penetration of the asphalt binder is decreasing with increasing the polymer percentage, where the optimum percentage of concentration is 7% SBR and 9% LDPE, but the penetration has a decreasing trend. It can be seen from Table 4 that the increase of SBR from 3 to 7% causes a reduction in the penetration from 44 to 34 dmm, while the penetration decreases from 40 to 26 dmm, when the LDPE increased from 3 to 9%. These results are in agreement with the findings of Babagoli (2021) and Che et al. (2022). Consequently, modified asphalt has a higher softening point and a lesser penetration than polymer-modified asphalt, showing that asphalt modification is more effective for improving the high temperature properties of asphalt binders.

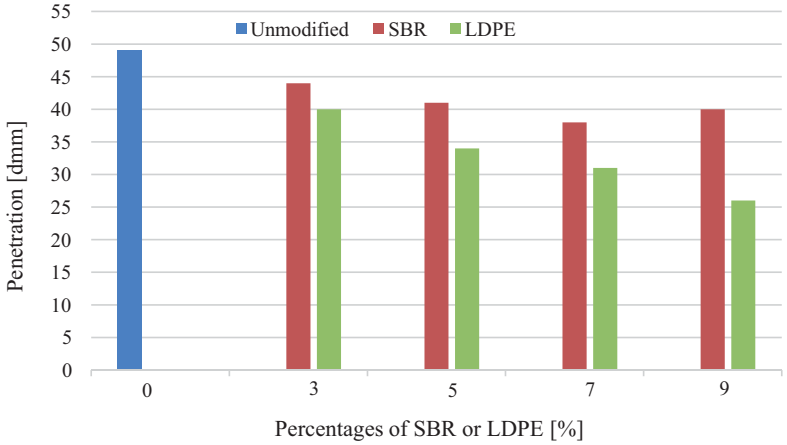

FIGURE 3. Penetration of asphalt with various styrene butadiene rubber (SBR) or low-density polyethylene (LDPE) contents

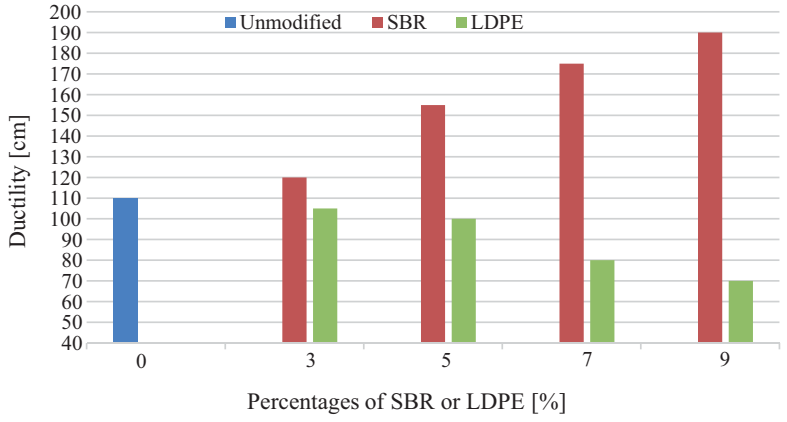

FIGURE 4. Ductility of asphalt with various styrene butadiene rubber (SBR) or low-density polyethylene (LDPE) contents

Regarding the ductility, it can be seen that when the concentration of LDPE increases from 3 to 9%, the ductility of the material decreases from 105 to 70 cm. It is worth noting that when a higher percentage of LDPE is used, the ductility drops rapidly; nevertheless, when the percentage of SBR increases, the ductility begins to rise. The ductility increased from 110 to 190 cm when the SBR increased from 3 to 9% (Fig. 4). This could be due to modifications in asphalt structures, which have made the asphalt more ductile. When the SBR concentration is raised, the rubber particles can form interconnections, making the asphalt less stiff and resulting in enhanced ductility; finally, the extra SBR introduces more elasticity, resulting in increased ductility.

The last row in Table 4 shows the penetration index (*PI*), and it is a developed relationship between the penetration and the softening point degree of the asphalt binder sample at 25°C. Through it, the sensitivity of the asphalt material and its impact on temperature are identified, and it can be calculated from the following mathematical relationship (Pfeiffer & Van Doormaal, 1936; Whiteoak et al., 2003).

$$\frac{20 - PI}{10 + PI} = 50\left[\frac{\log 800 - \log Pen.}{TRB - T}\right],$$

where:

PI – penetration index,
Pen. – penetration degree of the asphalt sample,
TRB – softening point is measured by the ring and ball method,
T – temperature at which penetration is measured is 25°C.

Increasing the *PI* of the asphalt binder remarkably enhances resistance to deformation of asphalt pavement, and the smaller the *PI* means the more sensitive the asphalt binder is to temperature variations. Asphalt binder specimens with standard specifications suitable for use in the field of paving (Tables 5 and 6) have *PI* values ranging from –2 to +2 (Hobson & Pohl, 1973). In this study, all the values of the *PI* are within the limits and range between +2 and –1. This indicates that meaning that the thermal stability of the product increases. The penetration index is illustrated in Figure 5.

TABLE 5. Rheological properties of asphalt binder (40–50) used in pavement according to the Iraqi specification SORB/R9 (State Commission of Roads and Bridges, 2003)

Property	Type 1	Type 2
	min	max
Softening point (R&B) [°C]	40	50
Penetration at 25°C [dmm]	51	62
Ductility [cm]	100	–

TABLE 6. Rheological properties of asphalt binder used in waterproofing and the field of flattening according to Iraqi specification IQS 1196 (Central Organization for Standardization and Quality Control [COSQC], 1988)

Property	Type 1		Type 2	
	min	max	min	max
Softening point (R&B) [°C]	57	66	70	80
Penetration at 25°C [dmm]	18	60	18	40
Ductility [cm]	100	–	30	–

Mustafa, S., Hameed, M. A., Dulaimi, A. (2022). Evaluation of the properties of modified local asphalt binder by using styrene butadiene rubber (SBR) or low-density polyethylene (LDPE). *Sci. Rev. Eng. Env. Sci.*, *31* (3), 190–202. DOI 10.22630/srees.3375

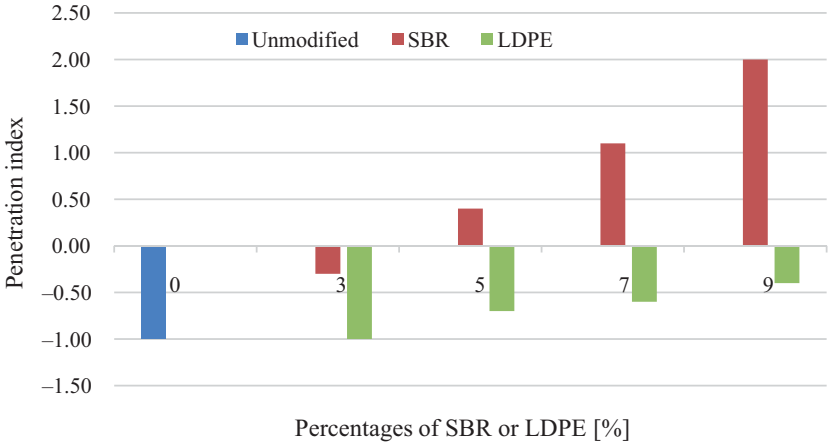

FIGURE 5. Penetration index of asphalt with various styrene butadiene rubber (SBR) or low-density polyethylene (LDPE) contents

Conclusions

1. The use of polymers such as SBR or LDPE affects the rheological property modification. Conventional asphalt binder testing results displayed that the addition of SBR or LDPE polymers increased the stiffness of the asphalt binder and reduced its temperature susceptibility. However, the degree of modification was more evident on asphalt binder residues, containing greater amounts of polymer SBR and depending on the valuable penetration index. The rheological properties of the asphalt modified with SBR or LDPE are mainly dependent on the SBR or LDPE content.
2. The polymers improved the rheological characteristics of the asphalt binder significantly and the improvement increased with polymer content but varied with polymer type. The modified local asphalt binder demonstrates that the effect of SBR or LDPE on the rheological properties of the asphalt at intermediate and high temperatures has been improved.
3. When SBR increased from 3 to 9%, the softening point improved by around 27%. While the increase in LDPE from 3 to 9% caused the softening point to rising from 53° to 60°C. This demonstrates that SBR performs better than LDPE at the same content (9%). Additionally, LDPE decreases the penetration of asphalt binder values of the emulsion residues considerably; although; their ductility properties begin to decrease slowly.
4. Both SBR and LDPE performs well in the improvement of the high-temperature performance of asphalt binders. Adding SBR or LDPE can improve the penetration index of asphalt binders leading to improve thermal stability. The behaviour of the two polymers showed that SBR had a higher penetration index,

this means the asphalt binder is less sensitive to temperature changes.

5. The penetration of asphalt is decreasing with increasing the polymer percentage, where the optimum percentage of concentration is 7% SBR and 9% LDPE, but the penetration has a decreasing trend. It can be seen from Table 4 that the increase of SBR from 3 to 7% causes a reduction in the penetration from 44 to 34 dmm, while the penetration decreases from 40 to 26 dmm when the LDPE increased from 3 to 9%.
6. The optimal percentage of concentration in terms of the penetration test is 7% SBR and 9% LDPE. The penetration of the asphalt binder decreases as the polymer percentage increases. The increase of SBR to 7% results in a reduction in penetration to 34 dmm, while increasing LDPE to 9% results in a decrease in penetration to 26 dmm.
7. One of the greatest methods to give solution to reduce the frequency of maintenance required at certain places is to employ a modified asphalt binder, which provides a substantially longer service life for maintenance treatments at problematic sites.

The next step for all sectors of the Iraqi industry is to collaborate to gain a deeper knowledge of the material's potential to produce better, more cost-effective roads for the benefit of both the industry and the community as a whole in various projects.

References

Abbas, A. S. (2017). Temperature zoning of Iraq for asphalt mix design. *Journal of Engineering and Sustainable Development*, *21* (5), 54–63.

Abduljabbar, N., Al-Busaltan, S., Dulaimi, A., Al-Yasari, R., Sadique, M. & Nageim, H. A. (2022). The effect of waste low-density polyethylene on the mechanical properties of thin asphalt overlay. *Construction and Building Materials*, *315*, 125722.

Abed, A., Hamdou, H. & Ahmed, N. (2011). Rheological properties of Iraqi asphalt binders measured using superpave system and shell software. *Journal of Engineering*, *17* (4), 783–799.

Ahmed, N. Y. & Al-Harbi, A. S. M. (2014). Effect of density of the polyethylene polymer on the asphalt mixtures. *Journal of University of Babylon*, *22* (4), 674–683.

Al-Bana'a, J. (2010). *Effect of polymer type on the performance of modified asphalt paving mixture* (doctoral dissertaton, MSc thesis). Babylon: University of Babylon, College of Engineering.

Alghrafy, Y. M., El-Badawy, S. M. & Abd Alla, E. S. M. (2021). Rheological and environmental evaluation of sulfur extended asphalt binders modified by high- and low-density polyethylene recycled waste. *Construction and Building Materials*, *307*, 125008.

Al-Hadidy, A. & Yi-Qiu, T. (2009). Mechanistic approach for polypropylene-modified flexible pavements. *Materials & Design*, *30* (4), 1133–1140.

American Association of State Highway and Transportation Officials [AASHTO] (2013a). *Standard method of test for ductility of asphalt materials* (T 51-09). Washington: The American Association of State Highway and Transportation Officials.

American Association of State Highway and Transportation Officials [AASHTO] (2013b). *Standard method of test for softening point of bitumen (Ring-and-Ball Apparatus)* (T 53--09). Washington: American Association of State Highway and Transportation Officials.

American Association of State Highway and Transportation Officials [AASHTO] (2015). *Standard method of test for penetration of bituminous materials* (T 49-15). Washington: American Association of State Highway and Transportation Officials.

Ameri, M., Vamegh, M., Rooholamini, H. & Haddadi, F. (2018). Investigating effects of nano/SBR polymer on rutting performance

of binder and asphalt mixture. *Advances in Materials Science and Engineering*, *2018*, 5891963.

Babagoli, R. (2021). Laboratory investigation of the performance of binders and asphalt mixtures modified by carbon nano tube, poly phosphoric acid, and styrene butadiene rubber. *Construction and Building Materials*, *275*, 122178.

Cao, X., Wang, H., Cao, X., Sun, W., Zhu, H. & Tang, B. (2018). Investigation of rheological and chemical properties asphalt binder rejuvenated with waste vegetable oil. *Construction and Building Materials, 180*, 455–463.

Central Organization for Standardization and Quality Control [COSQC] (1988). *Bitumen used for flatness* (IQS 1196). Baghdad: Central Organization for Standardization and Quality Control.

Chakraborty, S., Kar, S., Dasgupta, S., Mukhopadhyay, R., Bandyopadhyay, S., Joshi, M. & Ameta, S. C. (2010). Study of the properties of in-situ sodium activated and organomodified bentonite clay–SBR rubber nanocomposites – Part I: Characterization and rheometric properties. *Polymer Testing*, *29* (2), 181–187.

Che, T., Pan, B., Li, Y., Ge, D., Jin, D. & You, Z. (2022). The effect of styrene-butadiene rubber modification on the properties of asphalt binders: aging and restoring. *Construction and Building Materials, 316*, 126034.

Chopra, T., Parida, M., Kwatra, N. & Chopra, P. (2018). Development of pavement distress deterioration prediction models for urban road network using genetic programming. *Advances in Civil Engineering*, *2018*, 1253108.

Company for Tire Industry (2021). *Physical properties and specification of SBR*.

Fang, C., Li, T., Zhang, Z. & Wang, X. (2008). Combined modification of asphalt by waste PE and rubber. *Polymer Composites*, *29* 10), 1183–1187.

Hameed, A., Al-Busaltan, S., Dulaimi, A., Kadhim, M. A. & Al-Yasari, R. (2021). Evaluating modified asphalt binder comprising waste paper fiber and recycled low-density polyethylene. *Journal of Physics: Conference Series*, *1973* (1), 012237.

Hardin, J. C. (1995). *Physical properties of asphalt cement binders.* Error! Hyperlink reference not valid. West Conshohocken: ASTM International.

Hobson, G. D. & Pohl, W. (1973). *Modern petroleum technology*. New York: John Wiley & Sons.

Johnston, J. B. & King, G. (2008). *Using polymer modified asphalt emulsions in surface treatments. A federal lands highway interim report.* Washington: Federal Highway Administration.

Kim, H. H., Mazumder, M., Lee, S. J. & Lee, M. S. (2018). Characterization of recycled crumb rubber modified binders containing wax warm additives. *Journal of Traffic and Transportation Engineering (English Edition)*, *5* (3), 197–206.

Liang, M., Xin, X., Fan, W., Zhang, J., Jiang, H. & Yao, Z. (2021). Comparison of rheological properties and compatibility of asphalt modified with various polyethylene. *International Journal of Pavement Engineering, 22* (1), 11–20.

McNally, T. (2011). *Polymer modified bitumen: properties and characterisation*. Philadelphia: Woodhead Publishing.

Mazumder, M., Siddique, A., Ahmed, R., Lee, S. J. & Lee, M. S. (2020). Rheological and morphological characterization of Styrene--Isoprene-Styrene (SIS) modified asphalt binder. *Advances in Civil Engineering*, *2020*, 8877371.

Ministry of Oil, Midland refineries company, Al-Daurah refinery (2021). *Physical properties of asphalt binder*. Baghdad.

Mostafa, A. E. A., Tawhed, W. M. F. & Elshahat, M. R. (2016). Performance assessment of asphalt pavement mix modified by nano--silica and nano-clay. *International Journal of Advanced Engineering and Nano Technology*, *3* (3), 7–11.

Najaf, E., Abbasi, H. & Zahrai, S. M. (2022). Effect of waste glass powder, microsilica and polypropylene fibers on ductility, flexural and impact strengths of lightweight concrete. *International Journal of Structural Integrity*, *13* (3), 511–533.

Najaf, E., Orouji, M. & Zahrai, S. M. (2022). Improving nonlinear behavior and tensile and compressive strengths of sustainable light-

weight concrete using waste glass powder, nanosilica, and recycled polypropylene fiber. *Nonlinear Engineering*, *11* (1), 58–70.

Navarro, F. J., Partal, P., Martinez-Boza, F. J. & Gallegos, C. (2010). Novel recycled polyethylene/ground tire rubber/bitumen blends for use in roofing applications: Thermo-mechanical properties. *Polymer Testing*, *29* (5), 588–595.

Nizamuddin, S., Jamal, M., Gravina, R. & Giustozzi, F. (2020). Recycled plastic as bitumen modifier: The role of recycled linear low--density polyethylene in the modification of physical, chemical and rheological properties of bitumen. *Journal of Cleaner Production*, *266*, 121988.

Orouji, M., Zahrai, S. M. & Najaf, E. (2021). Effect of glass powder & polypropylene fibers on compressive and flexural strengths, toughness and ductility of concrete: an environmental approach. *Structures*, *33*, 4616–4628.

Pfeiffer, J. P. & Van Doormaal, P. (1936). The rheological properties of asphaltic bitumens. *Journal of the Institute of Petroleum Technologists*, *22*, 414–440.

Polacco, G., Filippi, S., Merusi, F. & Stastna, G. (2015). A review of the fundamentals of polymer-modified asphalts: asphalt/polymer interactions and principles of compatibility. *Advances in Colloid and Interface Science*, *224*, 72–112.

Polacco, G., Stastna, J., Biondi, D. & Zanzotto, L. (2006). Relation between polymer architecture and nonlinear viscoelastic behavior of modified asphalts. *Current Opinion in Colloid & Interface Science*, *11* (4), 230–245.

Presti, D. L. (2013). Recycled tyre rubber modified bitumens for road asphalt mixtures: a literature review. *Construction and Building Materials*, *49*, 863–881.

Ren, S., Liang, M., Fan, W., Zhang, Y., Qian, C., He, Y. & Shi, J. (2018). Investigating the effects of SBR on the properties of gilsonite modified asphalt. *Construction and Building Materials*, *190*, 1103–1116.

Roque, R., Birgisson, B., Tia, M., Kim, B. & Cui, Z. (2004). *Guidelines for use of modifiers in superpave mixtures: executive summary and volume 1 of 3 volumes: evaluation of SBS modifier*. Retrieved from: https://trid.trb.org/view/697983 [accessed 03.08.2022].

Sadhu, S. & Bhowmick, A. K. (2004). Preparation and properties of styrene–butadiene rubber based nanocomposites: the influence of the structural and processing parameters. *Journal of Applied Polymer Science*, *92* (2), 698–709.

Singh, B., Tarannum, H. & Gupta, M. (2003). Use of isocyanate production waste in the preparation of improved waterproofing bitumen. *Journal of Applied Polymer Science*, *90* (5), 1365–1377.

Speight, J. G. (2016). *Asphalt Materials Science and Technology*. Boston: Butterworth-Heinemann.

State Commission of Roads and Bridges (2003). *General specification for roads and bridge. Hot-mix asphaltic concrete pavement* (SORB/R9). Baghdad: Ministry of Housing and Construction, Department of Planning and Studies.

State Company for Petrochemical Industry in Basrah City (2008). *Physical Properties and Specifications for HDPE and LDPE polymers*. Basrah: State Company for Petrochemical Industry in Basrah City.

Whiteoak, D., Read, J. & Hunter, R. N. (2003). *The Shell bitumen handbook* (5th ed.). London: ICE Publishing.

Zhang, F. & Yu, J. (2010). The research for high--performance SBR compound modified asphalt. *Construction and Building Materials*, *24* (3), 410–418.

Zhu, J., Birgisson, B. & Kringos, N. (2014). Polymer modification of bitumen: advances and challenges. *European Polymer Journal*, *54*, 18–38.

Summary

Evaluation of the properties of modified local asphalt binder by using styrene butadiene rubber (SBR) or low-density polyethylene (LDPE). The influence of styrene butadiene rubber (SBR) or low--density polyethylene (LDPE) polymers on the characteristics of local asphalt binder was analyzed to characterize the rheological properties. The results indicated that the

SBR or LDPE increased the softening point. The softening point was enhanced by around 35% when 9% of SBR was used in comparison to the unmodified asphalt, while there was a 15% increment when LDPE was used. The results also indicated that the SBR or LDPE decreased the penetration rate. The penetration decreases by around 36% when 9% of SBR is used compared to the neat asphalt, while a significant increment was 89% when 9% of LDPE is used. Additionally, when 9% SBR was employed, the ductility of the asphalt binder rose by roughly 73%, but 64% less ductility was seen when 9% LDPE was utilized. Finally, the addition of the additive has improved the penetration index, thus reducing the temperature sensitivity. Due to said above, SBR and LDPE are practical and promising modifiers that will be useful in enhancing the performance of the asphalt binder straightforwardly and efficiently.

Scientific Review Engineering and Environmental Sciences (2022), 31 (3), 203–222

Sci. Rev. Eng. Env. Sci. (2022), 31 (3) https://srees.sggw.edu.pl

ISSN 1732-9353 (suspended) eISSN 2543-7496 DOI 10.22630/srees.3897

Received: 14.08.2022
Accepted: 30.09.2022

Mahmoud Mohamed BADAWY[1] https://orcid.org/0000-0002-1099-100X
Suzan Ali A. MUSTAFA[2]✉ https://orcid.org/0000-0001-9647-2456
Atef Eraky BAKRY[3] https://orcid.org/0000-0002-7514-3677
Zagazig University, Faculty of Engineering, Egypt

BEHAVIOR AND FAILURE TRACKING OF STRUCTURAL ELEMENTS USING APPLIED ELEMENT METHOD

Key words: applied element method (AEM), numerical analysis, stiffness matrix, large deformation failure tracking

Introduction

Structural analysis numerical techniques have two categories, continuum method and discrete element method. The first upholds the well-known finite element method (FEM) (Tagel-Din & Meguro, 1999; Meguro & Tagel-Din, 2000, 2001). Joints in the FEM can identify major cracks, however the position and direction of fracture propagation must be specified prior to analysis application (Meguro & Tagel-Din, 1997, 2001, 2002). Observing structural failure behavior in this method is difficult. If the behavior is considerably non-linear in the FEM, plenty of issues arise. For example, it is exceedingly difficult or impossible to use the FEM to evaluate the behavior of materials that move from a continuum to a totally discrete condition, like the behavior of structures before and during failure (Tagel-Din & Meguro, 1999).

The second category is discrete element methods, which upholds the distinct element method (DEM) and the rigid body and spring model (RBSM). The DEM assumes that the objective materials are composed of discrete pieces and may represent discrete material behavior. The extended DEM (EDEM) was primarily used for constraining structural analysis, and is often used to model and re-contact structural components with extremely large deformations (Meguro & Tagel-Din, 2001). The RBSM analysis could not be done until the system is collapsed (Meguro

✉samustafa@eng.zu.edu.eg

Badawy, M. M., Mustafa, S. A. A., Bakry, A. E. (2022). Behavior and failure tracking of structural elements using applied element method. *Sci. Rev. Eng. Env. Sci.*, *31* (3), 203–222. DOI 10.22630/srees.3897

& Tagel-Din, 2000). The main drawback of these rigid element methods is that the simulation results are heavily influenced by the element shape, dimension, and arrangement (Meguro & Tagel-Din, 1997, 2001). Furthermore, in the small deformation condition, both methods are less accurate than the FEM (Meguro & Tagel-Din, 1997, 2001, 2002; Tagel-Din & Meguro, 2000a, 2000b). Based on the foregoing, it is possible to infer that the present methodologies are unsuitable for tracking whole structural behavior from zero to collapse within an appropriate time frame (Meguro & Tagel-Din, 2000).

Applied element method (AEM)

The applied element method (AEM) is a recently developed displacement method (Meguro & Tagel-Din, 1997, 2000; Tagel-Din & Meguro, 1999). The ability of AEM to follow the behavior of the structural failure at various phases is impressive. This comprises the application of load, elastic stage, fracture initiation and propagation, the yielding of reinforcement, non-linear behavior, large deformation condition, the separation and collision of elements, and energy dissipation during collision (Lupoae & Bucur, 2009; Tokal-Ahmed, 2009; Wibowo, Reshotkina & Lau, 2009; Gohel, Patel & Joshi, 2013; Eraky, Mustafa, & Badawy, 2021). This paper sheds some light on AEM as a vital technique of structural analysis. A MATLAB program was created to apply the AEM method on structural elements. Moreover, some other points will be highlighted, the verification of the proposed program, the parameters affecting the analysis results and tracking the elements failure. In AEM, the structure is split into small rigid elements interlinked by springs (Meguro & Tagel-Din, 1997; Gohel et al., 2013; Shakeri & Bargi, 2015). Superior to FEM is AEM, because it requires less degrees of freedom (DOFs). This reduces the amount of time and memory required for processing (Meguro & Tagel-Din, 2001). By correctly arranging the springs, any form may be modeled without increasing the computing work (Christy, Pillai & Nagarajan, 2020). To transmit normal and shear stress, AEM elements are linked by a series of normal and shear springs. Springs, by their characteristics, stresses, and strains, characterize a specific volume of the elements (Meguro & Tagel-Din, 2000; Gohel et al., 2013; Shakeri & Bargi, 2015; Christy, Pillai, & Nagarajan, 2018). A spring is disconnected when the stress exceeds the permitted limit. Following the location of such springs might reveal the fracture pattern. Therefore, the structure behavior and crack propagation may be assessed at all stages of loading. The AEM also enables easy modeling, rapid processing, and high accuracy of results (Meguro & Tagel-Din, 2000; Christy et al., 2018).

To analyze the structures in AEM, they are split into minor rigid elements. Normal and shear springs are used to link the two parts as in Figure 1 at a single point of contact. Three DOFs are used to analyze the elements in 2D while six DOFs are used in 3D. These degrees of freedom reflect the element's translations and rotations. For every pair of springs surrounding the element, the stiffness matrix is derived using a unit displacement at the center of the element, as well as the forces at the other DOFs are determined if they are restricted (Meguro & Tagel-Din, 1997; Shakeri & Bargi, 2015; Christy et al., 2018). The stiffness matrix size for each spring is 6×6. The stiffness

matrices of every spring surrounding each element are assembled to produce the total stiffness matrix. Equation (1) shows the upper-left fourth of the stiffness matrix. The element stiffness matrix in this formulation is given by the contact point location (distance L and angles ɵ and α), and the stiffness of normal and shear springs (Meguro & Tagel-Din, 1997). The AEM is quicker than FEM since it does not need the definition of shape functions or the integration methods to construct the stiffness matrix (Shakeri & Bargi, 2015). The FEM is mostly used to simulate structural components like frames and shells. Because neighboring elements are connected by their shared nodes, partial connections are not permitted, and hence element failure cannot be simulated (Tokal-Ahmed, 2009). Although AEM modeling is similar to FEM, the primary difference is the element combination. The separation of elements in AEM is simpler to simulate than in FEM due to the use of springs between the elements. When the size of the element's changes, a transition zone is necessary in FEM for transferring large elements from smaller elements, but not in AEM. This leads to many fewer elements as shown in Figure 2. Moreover, AEM employs springs to link two components on a section of the surface (rather than the entire surface), whereas FEM cannot model connection without utilizing a different meshing technique (Tagel-Din & Rahman, 2006; Tokal-Ahmed, 2009; Shakeri & Bargi, 2015), as shown in Figure 3. The AEM assumes that every normal and shear spring stiffness represents a distinct area of the connected elements. The location of springs across the element's edges shown in Figure 4. Spring stiffness is calculated using Equation (2) (Meguro & Tagel-Din, 1997; Lupoae & Bucur, 2009).

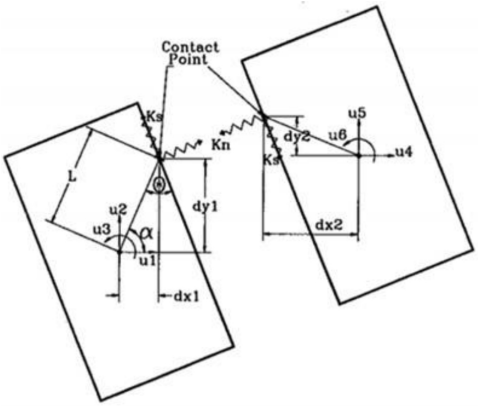

FIGURE 1. Element shape, contact point and degrees of freedom for two elements (Meguro & Tagel-Din, 1997)

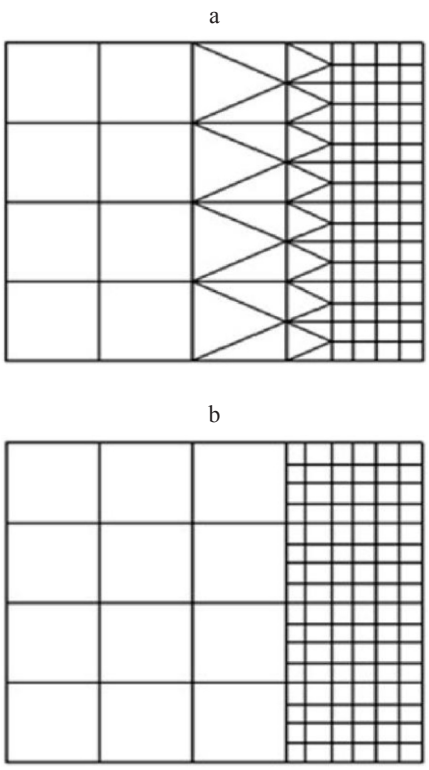

FIGURE 2. Transition from large elements to small elements in (a) FEM and (b) AEM (Shakeri & Bargi, 2015)

Badawy, M. M., Mustafa, S. A. A., Bakry, A. E. (2022). Behavior and failure tracking of structural elements using applied element method. *Sci. Rev. Eng. Env. Sci.*, *31* (3), 203–222. DOI 10.22630/srees.3897

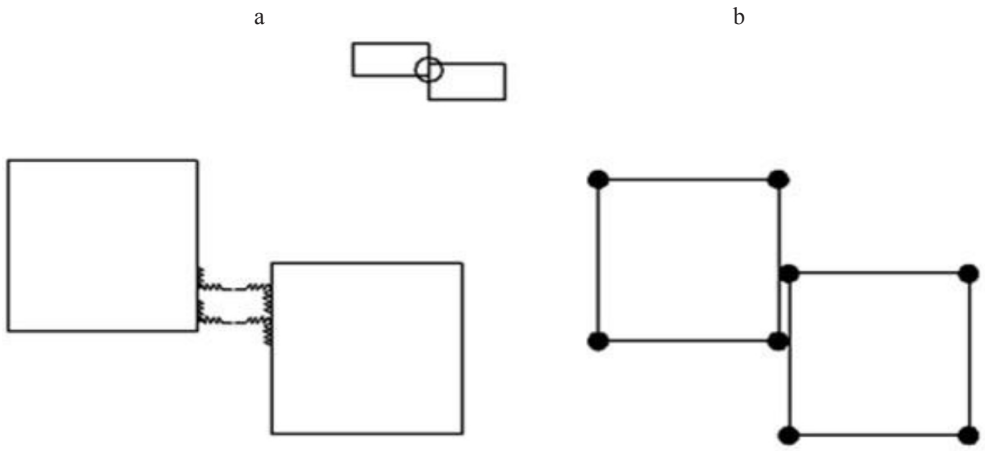

FIGURE 3. Element connectivity: a – AEM (connectivity via springs); b – FEM (no connectivity) (Shakeri & Bargi, 2015)

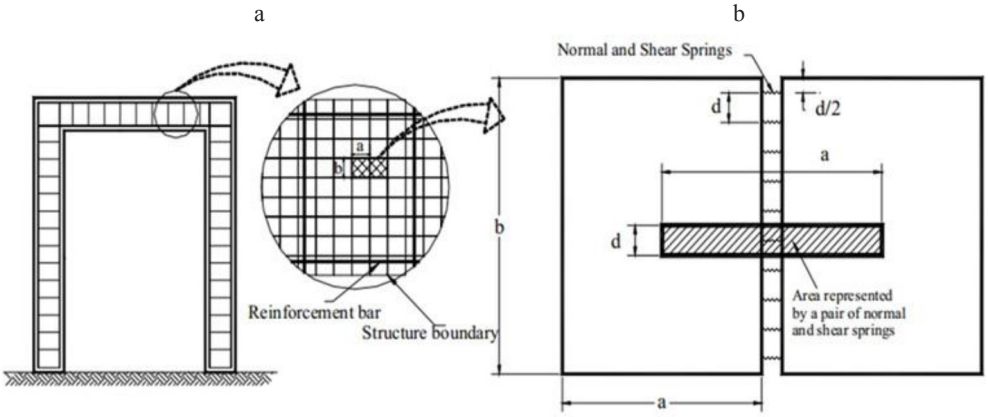

FIGURE 4. Modelling of structure in AEM: a – element generation; b – spring distributions and area of influence of each spring (Wibowo et al., 2009)

$$\begin{vmatrix} k_n \sin^2(\theta+\alpha) & -k_n \sin(\theta+\alpha)\cos(\theta+\alpha) & k_s L \sin(\alpha)\cos(\theta+\alpha) \\ +k_s \cos^2(\theta+\alpha) & +k_s \sin(\theta+\alpha)\cos(\theta+\alpha) & -k_n L \cos(\alpha)\sin(\theta+\alpha) \\ -k_n \sin(\theta+\alpha)\cos(\theta+\alpha) & k_s \sin^2(\theta+\alpha) & k_n L \cos(\alpha)\cos(\theta+\alpha) \\ +k_s \sin(\theta+\alpha)\cos(\theta+\alpha) & +k_n \cos^2(\theta+\alpha) & +k_s L \sin(\alpha)\sin(\theta+\alpha) \\ k_s L \sin(\alpha)\cos(\theta+\alpha) & k_n L \cos(\alpha)\cos(\theta+\alpha) & k_n L^2 \cos^2(\alpha) \\ -k_n L \cos(\alpha)\sin(\theta+\alpha) & +k_s L \sin(\alpha)\sin(\theta+\alpha) & +k_s L^2 \sin^2(\alpha) \end{vmatrix} \quad (1)$$

$$k_n = \frac{\mathrm{E} \cdot d \cdot t}{a}, k_s = \frac{\mathrm{G} \cdot d \cdot t}{a}, \quad (2)$$

where:

k_n – normal spring stiffness,
E – Young modulus of the concrete,
d – distance between the linked springs,
T – element's thickness,
a – representative area,
k_s – shear spring stiffness,
G – shear modulus of the concrete.

Proposed MATLAB open source program for AEM

A 2D MATLAB open source program was created to analyze various structures with varying boundary conditions using the AEM method and to permit researchers for enhancing the method. Figure 5 depicts the flow chart for the proposed program. The program's operation consisted of three steps: preparation, processing, and post-processing (Karad & Patel, 2020).

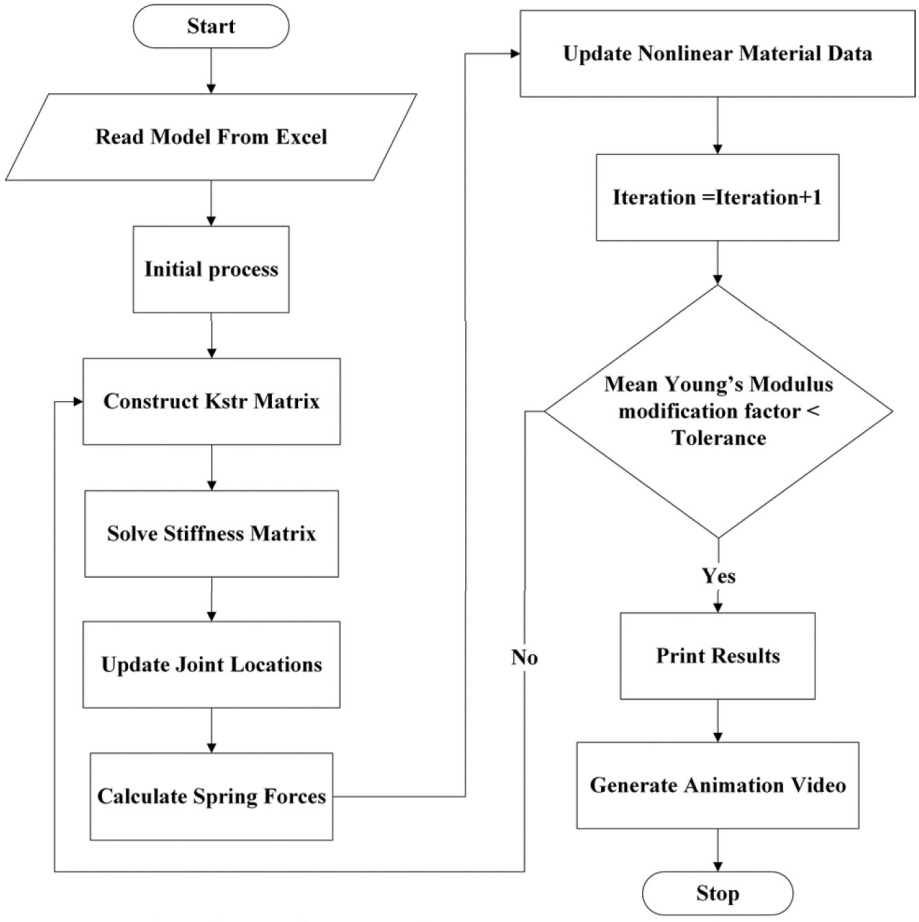

FIGURE 5. Flowchart of proposed MATLAB program for AEM

Badawy, M. M., Mustafa, S. A. A., Bakry, A. E. (2022). Behavior and failure tracking of structural elements using applied element method. *Sci. Rev. Eng. Env. Sci.*, *31* (3), 203–222. DOI 10.22630/srees.3897

The MATLAB was chosen for its capacity to handle large matrix multiplication, its robust programming language, and its converting functions and scripts into machine code that run efficiently.

Verification of the proposed program

The proposed program described in the preceding section was used to simulate various structural elements in verifying its precision and applicability. Various boundary conditions and loading were used on these structural elements. The verification was mostly based on stress and deformation values. Two scenarios were used to verify the program: linear static and non-linear geometric analysis in the case of large deformation. Using the MATLAB program in linear static analysis, three problems were used to verify the AEM method.

Cantilever beam

The first verified model was a cantilever beam, presented by (Meguro & Tagel-Din, 2000). This beam was also verified by Moss (2020). It was a six-meter long cantilever beam loaded by a concentrated force at its tip, as shown in Figure 6. The beam cross-section was 0.25 × 1.0 m. The modulus of elasticity was taken 840 MPa. The considered value of Poisson ratio was 0.15. Both studies concerned how mesh discretization affects solution precision. The same scenario was utilized using the proposed program. Many square mesh sizes were applied revealing meshes ranged from 1.0 × 1.0 to 0.083 × 0.083 m. In all cases, 10 linked springs were installed between the edges of the elements. Figure 6 shows the beam model with the lowest mesh size (0.083 m).

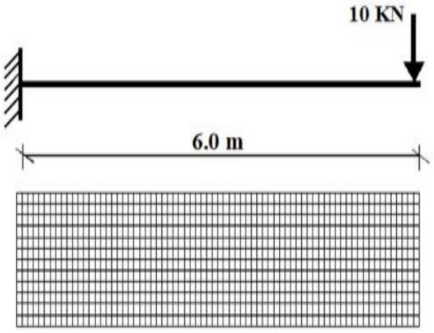

FIGURE 6. Cantilever beam with a point load on the free end and meshing

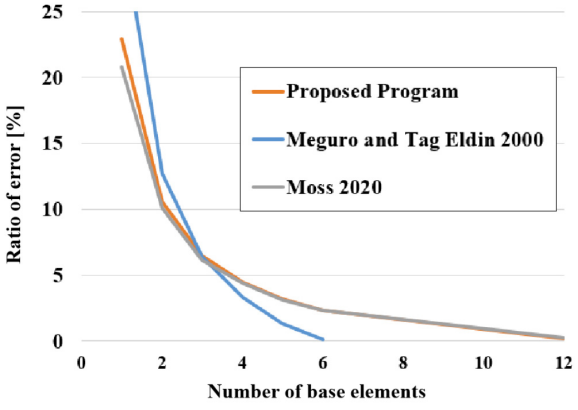

FIGURE 7. Accuracy of deflection of a cantilever beam with different mesh sizes

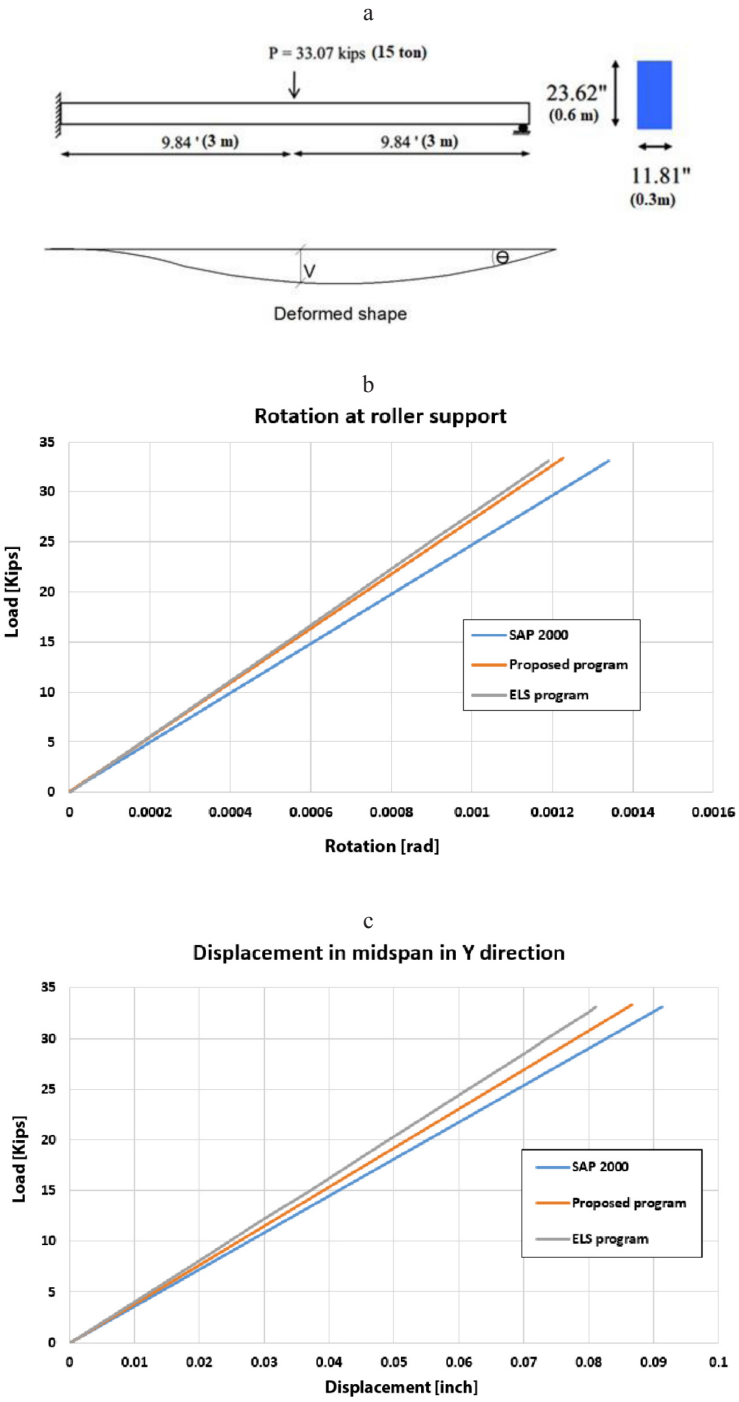

FIGURE 8. Results of proposed program, ELS and SAP2000 model: a – loading and geometry of the beam; b – load–deflection relation; c – load–rotation relation at the hinged support

Badawy, M. M., Mustafa, S. A. A., Bakry, A. E. (2022). Behavior and failure tracking of structural elements using applied element method. *Sci. Rev. Eng. Env. Sci.*, *31* (3), 203–222. DOI 10.22630/srees.3897

The obtained tip deflection of the beam was compared with the deflection computed using Euler–Bernoulli beam theory. The deviation of the proposed program's outcomes from theory was calculated as (error percentage), as were the deviations of both of these two previous programs (Meguro & Tagel-Din, 2000; Moss, 2020). Figure 7 displays the solution's convergence by charting the expected percent difference for every mesh size.

The deflection caused by the course meshes clearly resulted in substantial inaccuracy. Using a finer mesh, helped to eliminate the error. It is also clear that the proposed program's outcomes closely match those of Moss (2020).

Fixed-roller beam

The second problem used for verifying the linear static analysis was modeled using the Extreme Load Structures (ELS) software help (Extreme Load Analysis (ELS) Program, 2021). A six-meter long fixed roller beam was subjected to a static linear analysis. As illustrated in Figure 8, a concentrated force was applied at mid-span. The dimensions and material properties were maintained the same for the sake of comparison. The beam cross-section was 11.81 × 23.62 inch (0.3 × 0.6 m). The modulus of elasticity considered was 3,499.35 ksi. The value of Poisson ratio was 0.25.

The mid-span deflection and the rotation at the roller support were computed with the proposed AEM program, and elementary beam theory. Moreover, a finite element (FE) model analysis was performed using SAP2000 software. The proposed program's findings were also compared to the available ELS results. Figure 8 depicts the load––deflection and load–rotation relationships at the mid-span and roller support. When compared to other programs and the beam theory, the proposed program revealed in satisfactory results.

Fixed-fixed beam

The proposed program was verified using a third problem that is a fixed-fixed supported beam. The model was verified using the problem presented by Christy et al. (2018). As illustrated in Figure 9, a 5 kN concentrated force was applied at mid-span. The dimensions and material properties were maintained the same for the sake of comparison. The beam cross-section was 0.2 × 0.4 m. The modulus of elasticity considered was 25,000 kN·m^{-2}. The value of Poisson ratio was 0.2. The beam was split into 120 square elements, with five springs to investigate the deflection at 400 mm distant from the point load. The MATLAB code, FEM using SAP2000, and the beam theory were used to determine the deflection.

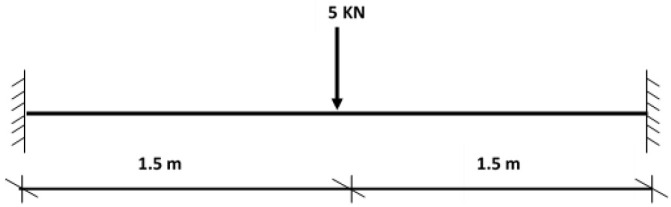

FIGURE 9. Fixed-fixed beam with center point load

The theoretical value of the deflection was 0.02624 and the calculated values from the proposed program and SAP2000 were 0.02506 and 0.0264 m respectively. The bending moment at mid-span was also calculated. The theoretical value of the moment was 1.875 kN·m^{-1}, while the calculated moment from SAP2000 was 1.877 kN·m^{-1} and from the proposed MATLAB program was 1.81 kN·m^{-1}. In comparison to the elementary beam theory and the SAP2000 software, the proposed program produced reasonable results.

Verification of large deformation static analysis

The proposed program was utilized to model a large deformation static analysis program (Meguro & Tagel-Din, 2002). A 12-meter simply supported beam was subjected to a steadily increasing point load at mid-span of the beam. The beam cross-section was 1 × 1 m. The modulus of elasticity considered was 210 MPa, and the Poisson ratio was 0.2. The verified beam's mesh discretization was 0.2 × 0.2 m. Figure 10 shows the beam's undeformed deformed shapes. The large deformation of the beam can be seen in the arched shape and the slipping of the roller towards to the loading point. The arching curvature of the beam indicates its increasing stiffness under load. The proposed program's load–displacement response was verified using the FE software ABAQUS.

In Figure 11, the maximum vertical deformation and the horizontal displacement at the roller support were plotted against the steadily rising load.

Both models' vertical displacement curves showed good agreement. The highest difference was 7.57%. While the horizontal displacement values were similar until roughly one-third of the maximum applied force. As the load level increased, the disparity between the two models' values increased, as indicated in Figure 11. This might be due to the ABAQUS program's distortion control, as well as the fact that local element deformation happened in the FE model but not in the proposed AEM model. This might results in discrepancies in the behavior of the two models, especially at high degrees of large deformation.

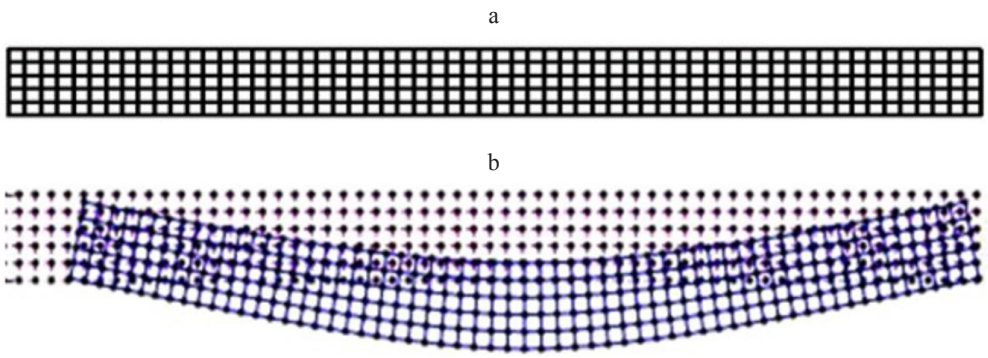

FIGURE 10. Large deformation static analysis model: a – 120 elements of 0.1 × 0.1 mesh; b – deformed shape

Badawy, M. M., Mustafa, S. A. A., Bakry, A. E. (2022). Behavior and failure tracking of structural elements using applied element method. *Sci. Rev. Eng. Env. Sci.*, *31* (3), 203–222. DOI 10.22630/srees.3897

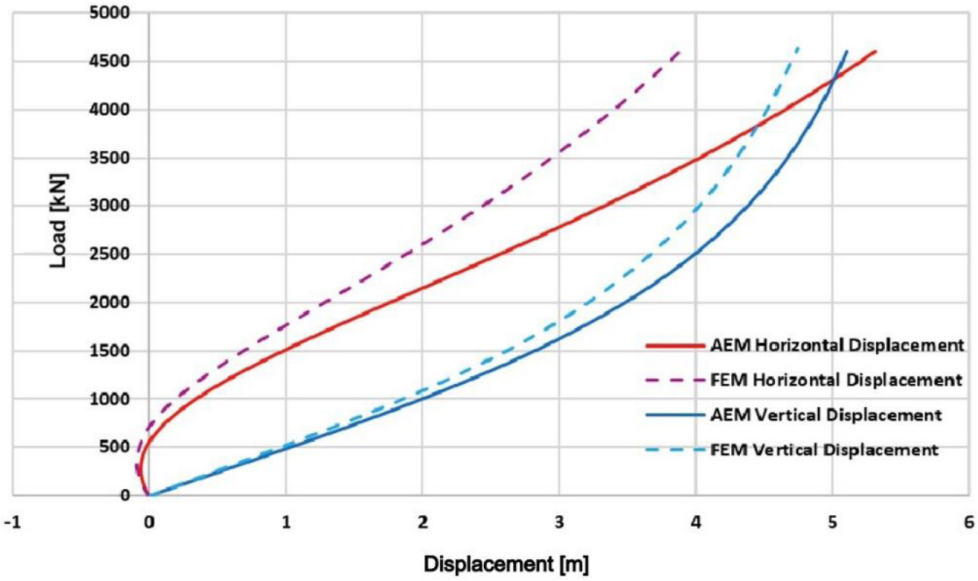

FIGURE 11. Load–displacement curves for AEM and FE models in large deformation static analysis problem

Parametric analysis

Some parameters were investigated to improve the proposed program's effectiveness in modelling various sorts of structures under various loading schemes. The size of elements and the number of connecting springs between the elements were the most effective ones. These two parameters were studied using a simply supported beam and a portal frame.

Simply supported beam

A three-meter long simple beam with cross section 0.2 × 0.45 m was subjected to two types of loading to study the effect of the size of elements and the number of sprigs connecting each pair on the modeling results. As illustrated in Figure 12, the first type of loading was a mid-span concentrated load of 60 t, while the second was two loads of 30 t at 0.9 m from the supports. The modulus of elasticity considered was $2.2 \times 106\ t \cdot m^{-2}$, and Poisson ratio was 0.2. The beams in the two cases were divided into 20, 60 and 240 square elements, to study the effect of increasing the number of elements (finer mesh size) on the proposed program outcomes. Meanwhile, each two elements in each trial were connected together by using three, five, seven and nine springs, to check the impact of using different number of springs on the proposed program results. This resulted in using 12 models to study these two parameters. The result concerning the simple beam with one concentrated load at mid-span were displayed in Figure 12. These results were compared to the calculated theoretical maximum displacement at mid-span. It can be noticed that, increasing the number of elements which were used in meshing the beam increased the accuracy of the program. The difference between the

proposed model and the theoretical calculation decreased to 0.65% which is considered a very good result. It is worthy note that the number of the connecting springs has a slight effect on the results. However, in case of the finest mesh, there was no effect of the different number of theses springs on the results, as can be seen in Figure 12.

The other loading scheme: four-point-bending was analyzed under the effect of the same two parameters as well. The second beam was divided into the same numbers of elements; 20, 60 and 240. More even, the different number of springs was utilized between the elements as well. The conclusion was noticed under this loading scheme. Figure 13 shows the maximum deflection of the beam for the different element numbers and springs. The finer the mesh, the more accurate results were obtained compared to the theoretical value of the maximum vertical deflection. The accuracy of the proposed program reached 97.4%.

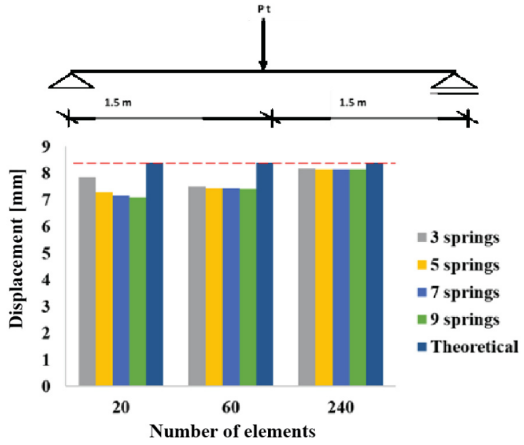

FIGURE 12. Effect of element size and number of connecting springs on the results of the simple beam under three-point bending

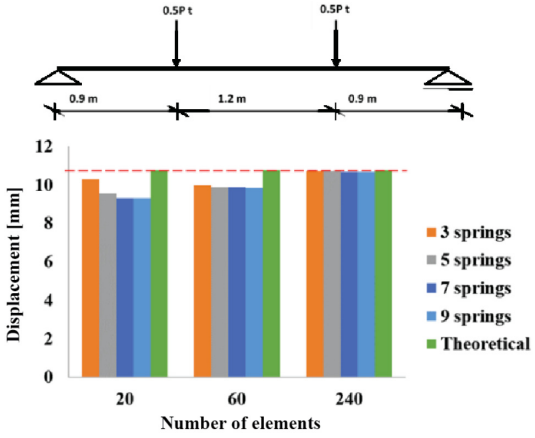

FIGURE 13. Effect of element size and number of connecting springs on the results of the simple beam under four-point bending

Badawy, M. M., Mustafa, S. A. A., Bakry, A. E. (2022). Behavior and failure tracking of structural elements using applied element method. *Sci. Rev. Eng. Env. Sci.*, *31* (3), 203–222. DOI 10.22630/srees.3897

Figure 13 illustrates the effect of the number of springs on the model accuracy. The difference between the results using different number of springs almost vanished in case of using a fine mesh.

Portal frame

A portal frame with the shown dimension in Figure 14 loaded by a horizontal lateral load was analyzed. The dimensions of the beam and columns cross-section were 0.3 × 0.6 m. The considered modulus of elasticity was 25 GPa. The Poisson ratio was 0.15. The frame was divided into different number of elements to represent the fineness of the mesh. The used element size were 30, 150, 100 and 50 mm revealing to number of elements as 64, 256, 576 and 2,304 elements as shown in Figure 15. Each two adjacent elements were connected by using three, five, seven and nine springs, to examine its effect on the frame results.

Figure 16 shows the results of these parameters; represented as maximum lateral displacements, compared to the calculated theoretical value. The figure shows that the difference between the proposed model decreases with the increase of the number of the elements. The difference decreased to 4.1%. It was noticed that using different numbers of springs affected the accuracy in case of coarse meshes. However, using small element size in the fine meshes, as in the last two cases, revealed in decreasing the effect of the number of springs used between each two adjacent elements.

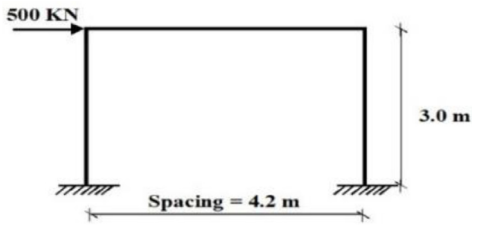

FIGURE 14. Portal frame exposed to point lateral load at top

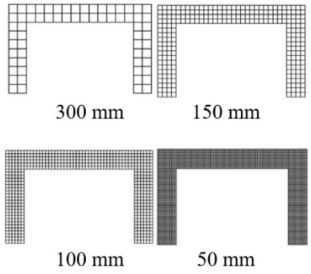

FIGURE 15. Structure discretization with different element size

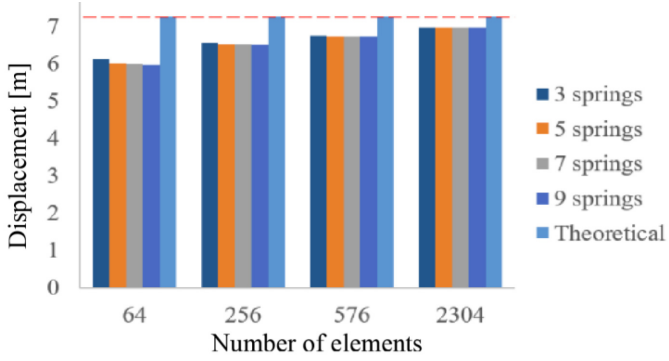

FIGURE 16. Effect of element size and number of connecting springs on the results of the portal frame with lateral load

It was noticed as well that using lower number of springs had a high precision on the processing time of the program. So, it is recommended to use fine mesh as possible with small number of springs to obtain accurate results with reasonable run time.

Failure tracking

An important feature was added to the proposed applied element program, which is the ability to track the failure in a loaded structure. This feature depended mainly on calculating the principal stress in each element during the incremented loading procedure (step by step loading). Failure was considered when the calculated principal stress reaches the specified ultimate stress according to the material type. The program was set so that each represented element whose stress reaches the ultimate tensile stress is colored in blue. While the element whose stress reaches the ultimate compressive stress is colored in red. After the on-set of failure, the failed elements' effect on the global stiffness matrix of the structure is omitted. In addition, the deformed shape at each load step could be extracted giving a motion of the structure. These features were applied on three different structures to show how the failure was tracked.

Cantilever beam

A three-meter long cantilever beam subjected to an incremental load on the free end was studied using the proposed program to track the failed elements and its spread. The cross-section of the beam was 0.2 × 0.6 m. The elasticity modulus used was 21.5 GPa. The Poisson ratio was 0.2. In each step, the increment was raised by 0.5 t. Figure 17a depicts the failure tracking. When the load reached 7 t, the first failed element was detected. Since the stress in this element exceeded the tensile strength. This can be seen by the user since the failed element is colored by blue in this case. By increasing the load, the failed elements increased.

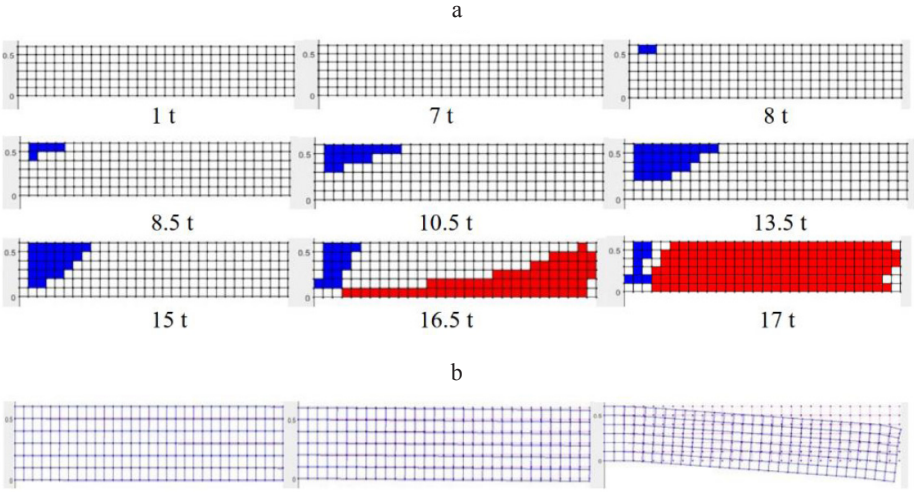

FIGURE 17. Results of cantilever beam: a – tracking of failed elements in a cantilever; b – deformed shape at different load steps of a cantilever beam

Badawy, M. M., Mustafa, S. A. A., Bakry, A. E. (2022). Behavior and failure tracking of structural elements using applied element method. *Sci. Rev. Eng. Env. Sci.*, *31* (3), 203–222. DOI 10.22630/srees.3897

The colored elements increased then it was noticed that after a load of 16 t crushed elements started to appear and were colored by red, as shown in the figure. The deformed shape can be obtained as a result from the program as well. The motion of the deformed shape was obtained, and Figure 17b shows the deformed shape at different load steps.

Simply supported beam

A three-meter long simply supported beam subjected to an incremental load at mid-span of the beam was studied using the proposed program to follow the failure, start and spread. The cross-section of the beam was 0.2 × 0.45 m.

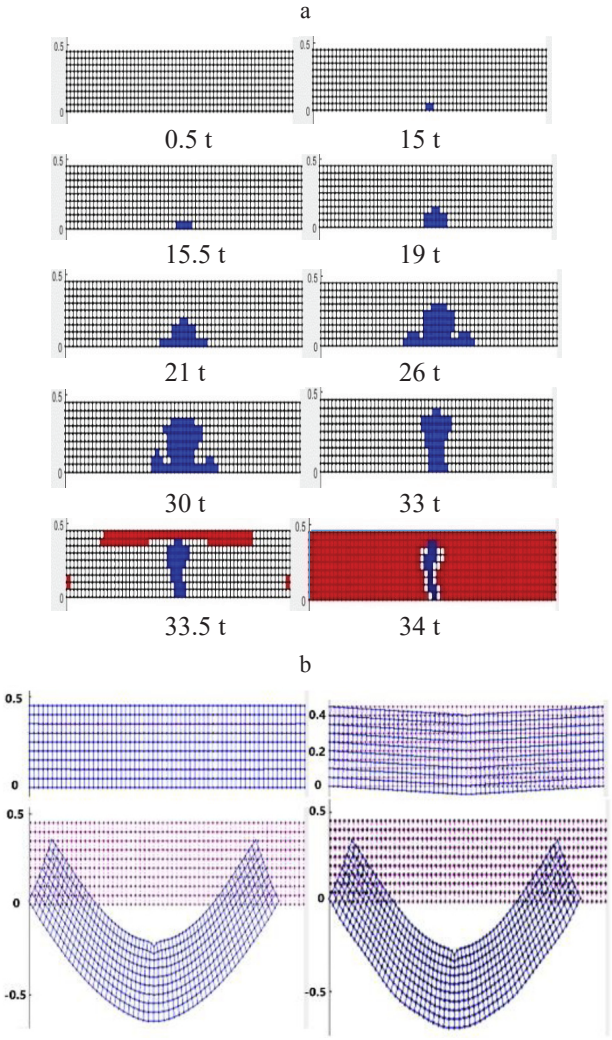

FIGURE 18. Results of simply supported beam: a – tracking of the failed elements of simply supported beam under mid-span concentrated load; b – deformed shape at different load steps of a simply supported beam

The elasticity modulus used was 21.5 GPa. The Poisson ratio was found to be 0.2. In each step, the increment was raised by 0.5 t. Figure 18a depicts the failure tracking. When the load reached 15 t, the first failed element was depicted. The first element failed because it exceeded the tensile strength. The number of the failed elements in tension increased gradually with increasing the load, then the failed elements under compression started to show, as can be seen in the figure. As described above, the deformed shape at different load steps is shown in Figure 18b.

Portal frame

The proposed program was used to follow the failure initiation and propagation of a portal frame subjected to increased lateral load. The frame's dimensions are shown in Figure 19. Both the beam and the columns have cross-sectional dimensions of 300 × 600 mm. Young modulus was set to 25 GPa. The Poisson ratio had a value of 0.2. The element sizes used were 100 mm. Three springs were attached between each pair of adjacent elements. In each step, the value of the load (P) raised by 1 N. Figure 20 depicts the failure tracking. The first failed element was detected when it was surpassed the specified tensile strength.

With increasing the applied load, more elements in different positions of the frame reached the ultimate tensile strength. Therefore, these elements were colored to show the position of failed elements, as instructed in the proposed program. On the other hand, when the elements reached the specified ultimate compressive stress, the crushed elements were colored by red in the regions of compression. It was inferred from these results that the proposed program designed to use the AEM method could accurately anticipate the failure pattern.

Infilled frame

The proposed program was used to follow the failure initiation and propagation of an infilled frame subjected to increased lateral load. This was to examine applicability of the proposed program to model a structure composed of two different materials. The structure was a plain concrete frame infilled with a brick wall, as shown in Figure 21. Young modulus for concrete and bricks were 21.5 and 7 GPa, respectively (Nichols & Totoev, 1997). The Poisson ratio for concrete and bricks were 0.2 and

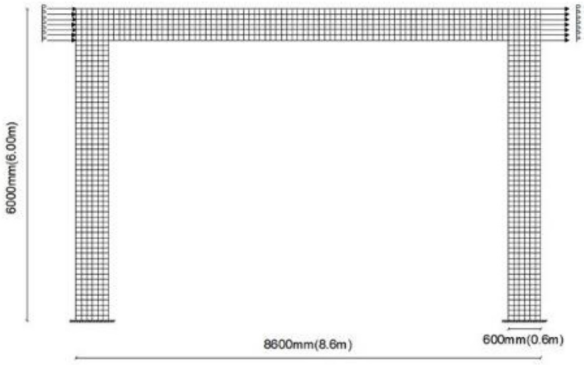

FIGURE 19. Portal frame under increased lateral loads

Badawy, M. M., Mustafa, S. A. A., Bakry, A. E. (2022). Behavior and failure tracking of structural elements using applied element method. *Sci. Rev. Eng. Env. Sci.*, *31* (3), 203–222. DOI 10.22630/srees.3897

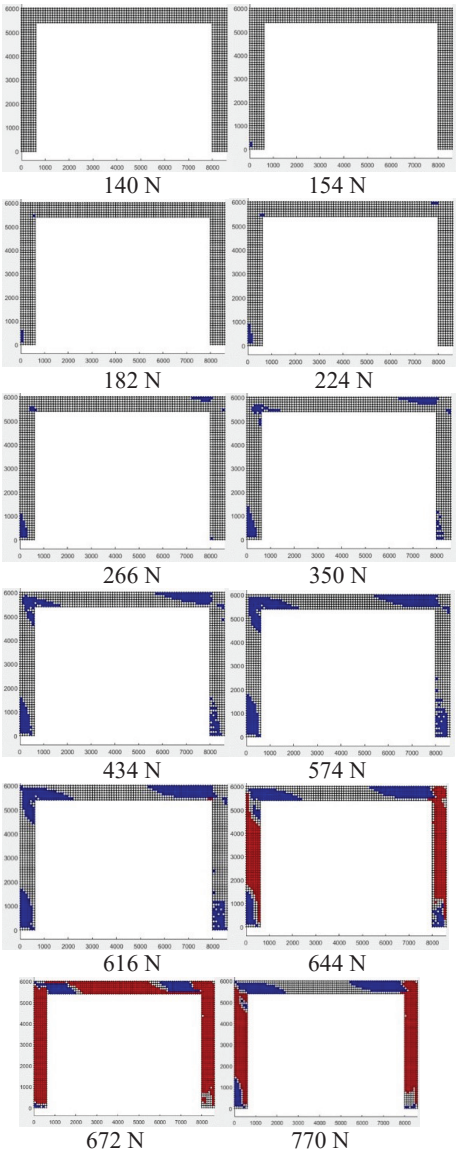

FIGURE 20. Results of portal frame with incremental lateral loads: tracking failed elements

0.21, respectively. The structure consisted of concrete frame supported by concrete ground beam and filled with bricks, with the dimensions shown in the figure. Both the beam and the columns have cross-sectional

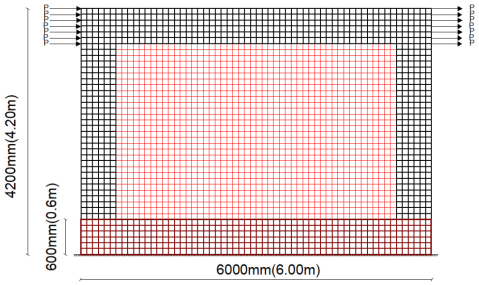

FIGURE 21. Infilled frame under increased lateral loads

dimensions of 250 × 600 mm, while the cross-sectional dimensions of ground beam are 400 × 600 mm. The width of bricks was 120 mm. The element size used were 100 mm, as seen in Figures 21, 22 and 23. Three springs were attached between each pair of adjacent elements. The applied load step size was 0.5 t to ease tracking the failed elements accurately. The first failed element was detected when it surpassed the permissible tensile strength of the bricks at the boundary between concrete and bricks, as shown in Figure 22.

On the other hand, when other elements reached the specified permissible compressive stress, the crushed elements were colored by red. Figure 23 shows the deformed shape of the infilled frame. It was inferred from these results that the proposed program designed to use the AEM method could accurately anticipate the failure pattern in the case of using two different materials.

Conclusions

Through the presented study in this research, the following conclusions were derived:

– Using AEM, the proposed program showed good accuracy in simulating different structural elements with different

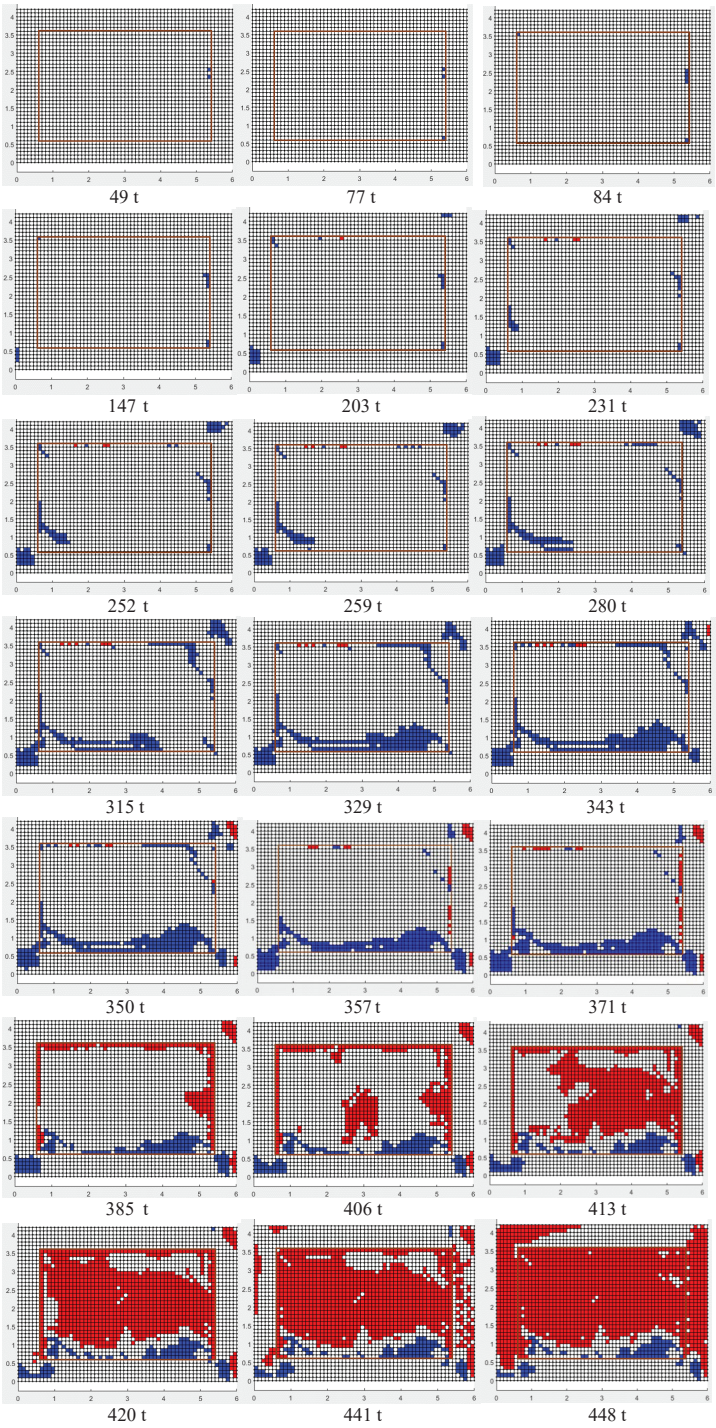

FIGURE 22. Results of infilled frames: tracking failed elements of an infilled frame

Badawy, M. M., Mustafa, S. A. A., Bakry, A. E. (2022). Behavior and failure tracking of structural elements using applied element method. *Sci. Rev. Eng. Env. Sci.*, *31* (3), 203–222. DOI 10.22630/srees.3897

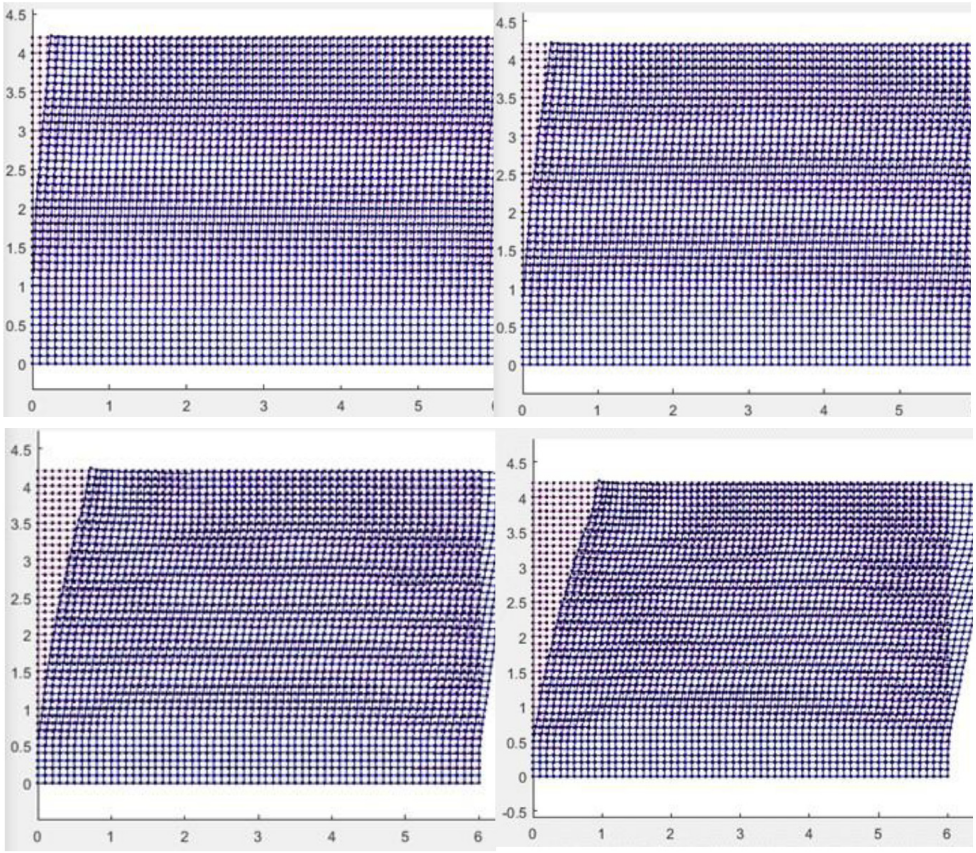

FIGURE 23. Results of infilled frames: deformed shape at different load steps

boundary conditions. The results were verified using available software packages, results computed using beam theory and previous examples from literature.

– More accurate results were obtained from increasing the number of elements in meshing a structure. However, increasing the number of springs between each two adjacent elements had a slight effect on the results.
– To achieve good results with a reasonable run time, fine mesh with a modest number of springs is advised.
– The proposed program managed to predict failure initiation and propagation during the different loading steps of the model unlike FE programs.
– When elements exceed the permissible tensile or compressive stresses, they were directed to be colored by two different colors, to differentiate the failure kind.

The proposed program could accurately represent failure propagation and deformation of a structure composed of more than one material.

References

Eraky, A., Mustafa, S. A. & Badawy, M. (2021). Structural analysis using Applied Element Method: a review. *Egyptian Journal for Engineering Sciences and Technology*, *34* (1), 16–27. https://doi.org/10.21608/eijest.2021.56786.1043

Extreme Load Analysis (ELS) *Program (2021). Linear analysis of a statically indeterminate beam*. Retrieved from: https://www.extremeloading.com/download/Static-Loading-Verification-Samples/Elastic-Cases/General/1-001.pdf [acccessed: 13.08.2022].

Gohel, V., Patel, P. V. & Joshi, D. (2013). Analysis of frame using applied element method (AEM). *Procedia Engineering*, *51*, 176–183. https://doi.org/10.1016/j.proeng.2013.01.026

Christy, D. L., Pillai, T. M. & Nagarajan, P. (2018). Analysis of concrete beams using applied element method. *IOP Conference Series: Materials Science and Engineering*, *330* (1), 012117. https://doi.org/10.1088/1757-899X/330/1/012117

Christy, D. L., Pillai, T. M. & Nagarajan, P. (2020). Annular Sector Element for Applied Element Method. *Journal of the Institution of Engineers (India): Series A*, *101* (4), 571–578. https://doi.org/10.1007/s40030-020-00455-3

Karad, P. & Patel, P. (2020). Analysis of reinforced concrete element using Applied Element Method (AEM). *Proceedings of the International Conference on Recent Advances in Computational Techniques*, *2020*, 1–5. https://doi.org/10.2139/ssrn.3697555

Lupoae, M. & Bucur, C. (2009). Building demolition – positive aspect of progressive collapse. *Military Technical Academy Review*, *19* (4), 399–408.

Meguro, K. & Tagel-Din, H. (1997). A new efficient technique for fracture analysis of structures. *Bulletin of Earthquake Resistant Structure Research Center*, *30*, 103–116.

Meguro, K. & Tagel-Din, H. (2000). Applied element method for structural analysis: theory and application for linear materials. *Structural Engineering/Earthquake Engineering*, *17* (1), 31–45.

Meguro, K. & Tagel-Din, H. (2001). Applied Element Simulation of RC Structures under cyclic loading. *Journal of Structural Engineering*, *127* (Nov.), 1295–1305.

Meguro, K. & Tagel-Din, H. (2002). Applied Element Method used for large displacement structural analysis. *Journal of Natural Disaster Science*, *24* (1), 25–34.

Moss, J. M. (2020). *Development, verification, and validation of an applied Element Method simulation framework for glass lite fracture, fragmentation, and debris field prediction* (doctoral dissertation). The University of North Carolina at Charlotte, Charlotte.

Nichols, J. & Totoev, Y. (1997). Experimental determination of the dynamic Modulus of Elasticity of masonry units. *15th Australian Conference on the Mechanics of Structures and Materials*, *2015*, 1–7.

Shakeri, A. & Bargi, K. (2015). Use of applied element method for structural analysis. *KSCE Journal of Civil Engineering*, *19* (5), 1375–1384. https://doi.org/10.1007/s12205-015-0625-4

Tagel-Din, H. & Meguro, K. (1999). Applied Element Method: a new efficient tool for design of structure considering its failure behavior. *5th US National Conference on Lifeline Earthquake Engineering*, *13*, 1–30.

Tagel-Din, H. & Meguro, K. (2000a). Analysis of small scale RC building subjected to shaking table tests using applied element method. *Proceedings of the 12th World Conference on Earthquake Engineering*, 1–8. Retrieved from: http://www.iitk.ac.in/nicee/wcee/article/0464.pdf [acccessed: 13.08.2022].

Tagel-Din, H. & Meguro, K. (2000b). Applied element method for dynamic large deformation analysis of structures. *Doboku Gakkai Ronbunshu*, *2000* (661), 1–10.

Tagel-Din, H. & Rahman, N. A. (2006). The Applied Element Method: the ultimate analysis of progressive collapse. *STRUCTURE Magazine*, *4*, 30–33.

Tokal-Ahmed, Y. M. (2009). *Response of bridge structures subjected to blast loads and protection techniques to mitigate the effect of blast hazards on bridges*. Rutgers-New Brunswick: The State University of New Jersey.

Wibowo, H., Reshotkina, S. S. & Lau, D. T. (2009). Modelling progressive collapse of RC bridges during earthquakes. *Proceedings, Annual Conference – Canadian Society for Civil Engineering*, *2*, 899–909.

Summary

Behavior and failure tracking of structural elements using applied element method. Applied element method (AEM) is a recently displacement-based structural analysis method. It provides the benefits of both the finite element method (FEM) and the discrete element method (DEM). This method relies on those structures are segmented into rigid elements linked by normal and shear springs. In this paper a brief note of the AEM is given. Then, using the AEM, a 2D MATLAB open source program was created to analyze different structures with varied boundary conditions and to permit researchers for enhancing the method. The proposed program was verified using linear elastic analysis and large deformation static analysis. The influence of element size and the number of connecting springs between elements was studied. Finally, the proposed program was capable of tracking failed elements and their spread. In addition, the program could predict deflection values and structure deformed shape.

Instruction for Authors

The journal publishes in English languages, peer-reviewed original research, critical reviews and short communications, which have not been and will not be published elsewhere in substantially the same form. Author of an article is required to transfer the copyright to the journal publisher, however authors retain significant rights to use and share their own published papers. The published papers are available under the terms of the principles of Open Access Creative Commons CC BY-NC license. The submitting author must agree to pay the publication charge (see Charges).

The author of submitted materials (e.g. text, figures, tables etc.) is obligated to restricts the publishing rights. All contributors who do not meet the criteria for authorship should be listed in an Acknowledgements section of the manuscript. Authors should, therefore, add a statement on the type of assistance, if any, received from the sponsor or the sponsor's representative and include the names of any person who provided technical help, writing assistance, editorial support or any type of participation in writing the manuscript.

Uniform requirements for manuscripts

The manuscript should be submitted by the Open Journal System (OJS) at https://srees.sggw.edu.pl/about/submissions. All figures and tables should be placed near their reference in the main text and additionally sent in a form of data files (e.g. Excel, Visio, Adobe Illustrator, Adobe Photoshop, CorelDRAW). Figures are printed in black and white on paper version of the journal (color printing is combined with an additional fee calculated on a case-by-case basis), while on the website are published in color.

The size of the manuscript should be limited up to 10 pages including overview, summary, references and figures (the manuscript more than 13 pages is unacceptable); Please set the text format in single column with paragraphs (A4 paper format), all margins to 25 mm, use the font Times New Roman, typeface 12 points and line spacing one and half.

The submitted manuscript should include the following parts:

- name and SURNAME of the author(s) – up to 5 authors
- affiliation of the author(s), ORCID Id (optional)
- title of the work
- key words
- abstract (about 500 characters)
- text of the paper divided into: Introduction, Material and Methods, Results and Discussion, Conclusions, References and Summary
- references in APA style are listed fully in alphabetical order according to the last name of the first author and not numbered; please find the details below
- post and mailing address of the corresponding author:

  Author's address:
  Name, SURNAME
  Affiliation
  Street, number, postal code, City
  Country
  e-mail: adress@domain

- Plagiarism statement (https://srees.sggw.edu.pl/copyright)

Reference formatting

In the Scientific Review Engineering and Environmental Sciences the APA 6th edition style is used.

Detailed information

More information can be found: https://srees.sggw.edu.pl